

Multivariable Isoperformance Methodology for Precision Opto-Mechanical Systems

Olivier L. de Weck*

Massachusetts Institute of Technology, Cambridge, MA 02139

David W. Miller†

Massachusetts Institute of Technology, Cambridge, MA 02139

and Gary E. Mosier‡

NASA Goddard Space Flight Center, Greenbelt, MD 20771

A novel approach to the design of complex, multi-disciplinary systems, such as space telescopes, is presented in the form of a multivariable isoperformance methodology. The isoperformance approach first finds a point design within a topology, which meets the performance requirements with sufficient margins. The performance outputs are then treated as equality constraints and the non-uniqueness of the design space is exploited by trading key design variables with respect to each other. Three algorithms (branch-and-bound, tangential front following and vector spline approximation) are developed for the bivariate and multivariable problem. The isoperformance approach attempts to avoid situations, where very difficult requirements are levied onto one subsystem, while other subsystems hold substantial margins. An experimental validation is carried out on a laboratory testbed, trading disturbance excitation amplitude and payload mass. The predicted performance contours match the experimental data very well at low excitation levels, typical of the disturbance environment on precision opto-mechanical systems. The relevance of isoperformance to space systems engineering is demonstrated with a comprehensive NEXUS spacecraft dynamics and controls analysis.

1 Introduction

IN designing complex high-performance technical systems there are typically two conflicting quantities that come into play: resources and system performance. One traditional paradigm fixes the amount of available resources (costs) and attempts to optimize the system performance given this constraint. The other approach is to constrain the system performance to a desired level and to find a design (or a family of designs) that will achieve this performance at minimal cost. This paper explores the second approach by developing a framework termed the “isoperformance methodology” for dynamic, linear time-invariant (LTI) systems. This is a framework, where the solutions to a design problem do not distinguish themselves by the performance they achieve, but rather by the “cost” and “risk” required to achieve this performance.

This framework is first developed generically for LTI systems, which can be described in state space form. It is then applied specifically to dynamics and controls problems of precision opto-mechanical systems, such

*Assistant Professor, Department of Aeronautics and Astronautics, Engineering Systems Division (ESD), Member.

†Associate Professor, Director, Space Systems Laboratory, Department of Aeronautics and Astronautics, Member

‡Systems Engineering Services & Advanced Concepts, Code 531, Member

Copyright © 2002 by the American Institute of Aeronautics and Astronautics, Inc. All rights reserved.

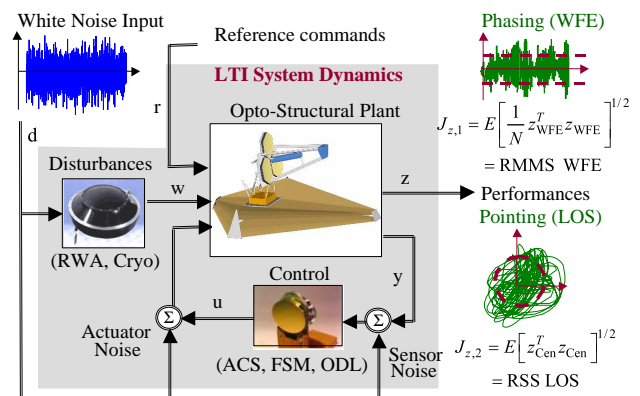


Fig. 1 Block diagram of science target observation mode of a space telescope.

as the next generation of space-based observatories. These systems combine structures, optics and control systems such that stringent pointing and phasing requirements can be met in the presence of dynamic disturbance sources. The typical problem setting is depicted in Figure 1.

Inputs are white-noise unit-intensity disturbances d and reference commands r . Outputs are opto-scientific metrics of interest z . The performances, J_z , are typically expressed in terms of the root-mean-square (RMS) of the outputs. The goal of a dis-

turbance analysis (= performance assessment) is to predict the expected values of the performances, $J_{z,i}$, where $i = 1, \dots, n_z$ and n_z is the number of performance metrics. This has been previously developed and demonstrated by Gutierrez.¹⁸

Oftentimes the number of parameters, n_p , for which a designer has to determine specific values exceeds the number of performance metrics n_z , i.e. $n_p - n_z \geq 1$. The traditional approach is to first choose reasonable numbers for the system parameters p_j , where $j = 1, \dots, n_p$, and to predict the resulting performances $J_{z,i}$ (initial performance assessment). If all or some of the predicted performances do not initially meet the specified requirements, $J_{z,req,i}$, including margins, a sensitivity analysis can provide partial derivatives $\partial J_{z,i} / \partial p_j$ which are used to identify in which direction important parameters p_j should be changed. This is intended to drive the system to a design point which satisfies all requirements, i.e. a condition where $J_{z,i} \leq J_{z,req,i}$ is true for all i . This is as far as most existing tools and methodologies will go in the design process.

Once a nominal design, p_{nom} , has been found that meets all requirements with sufficient margins, it is important to realize that this design is generally not unique. It is likely that different combinations of values for the system parameters, p_j , will yield the same predicted system performance $J_{z,i}$. It is the essential idea of isoperformance to find and exploit these performance invariant solutions, p_{iso} , in the design space. A formal process and specific tools are needed, which will ensure that a required performance level is met, while minimizing the cost and risk of the system. This is the impetus for the following problem definition.

Problem Definition

The primary objective of this paper is to develop a comprehensive multivariable isoperformance methodology for precision opto-mechanical systems. In other words, given the required system performances, $J_{z,req,i}$, where $i = 1, \dots, n_z$, attempt to find a set of independent solution vectors, $p_{iso} = [p_1, p_2, \dots, p_{n_p}]$, whose elements are the variable parameters p_j , such that an efficient system design can be achieved. This can be formulated mathematically as follows.

An appended state space representation of the dynamics of a closed-loop or open-loop linear time-invariant (LTI) system is given as

$$\begin{aligned} \dot{q} &= A_{zd}(p_j)q + B_{zd}(p_j)d + B_{zr}(p_j)r \\ z &= C_{zd}(p_j)q + D_{zd}(p_j)d + D_{zr}(p_j)r \end{aligned} \quad (1)$$

where A_{zd} is the state transition matrix, B_{zd} and B_{zr} are the disturbance and reference input coefficient matrices, C_{zd} is the performance output coefficient matrix, D_{zd} and D_{zr} are the disturbance and reference feedthrough matrices, d are unit-intensity white noise

inputs, r are reference inputs, z are system performance outputs, q is the state vector and p_j are the independent variable system parameters. Given that the functionals

$$J_{z,i}(p_j) = F(z) \text{ , e.g. } J_{z,i} = E [z_i^T z_i]^{1/2} \quad (2)$$

where $i = 1, 2, \dots, n_z$, are a definition of the performance metrics of interest, find a set of vectors, p_{iso} , such that the performance equality (isoperformance) constraint

$$J_{z,i}(p_{iso}) \equiv J_{z,req,i} \quad \forall i = 1, 2, \dots, n_z \quad (3)$$

is met, assuming that the number of parameters exceeds the number of performances

$$n_p - n_z \geq 1 \quad (4)$$

and that the parameters p_j are bounded below and above as follows:

$$p_{j,LB} \leq p_j \leq p_{j,UB} \quad \forall j = 1, 2, \dots, n_p \quad (5)$$

The isoperformance condition (3) has to be met subject to a numerical tolerance, τ

$$\left| \frac{J_z(p_{iso}) - J_{z,req}}{J_{z,req}} \right| \leq \frac{\tau}{100} \quad (6)$$

If scalar or vector (multiobjective) cost functions, J_c , and risk functions, J_r , are given, solve a constrained non-linear optimization problem such that

$$\begin{aligned} \text{MLP} \\ \min & [\eta J_c^T Q_{cc} J_c + (1 - \eta) J_r^T Q_{rr} J_r] \\ \text{such that } & p_{iso} \in \mathbf{I} \text{ and } p_{j,LB} \leq p_j \leq p_{j,UB} \\ \text{and } & \eta \in [0 \ 1] \end{aligned} \quad (7)$$

where the weight η is used to trade between cost and risk objectives and Q_{cc} and Q_{rr} are cost and risk weighting matrices respectively. The set \mathbf{I} is the performance invariant (isoperformance) set, containing only solutions satisfying (3).

Alternatively this can be formulated in terms of set theory. Figure 2 shows various sets in the vector space $p = [p_1 \ p_2 \ \dots \ p_{n_p}]^T$ and their mutual relationship in the general case¹.

¹The eigenvalues λ_i are obtained by solving the eigenvalue problem $[A_{zd} - \lambda_i I] \phi_i = 0$.

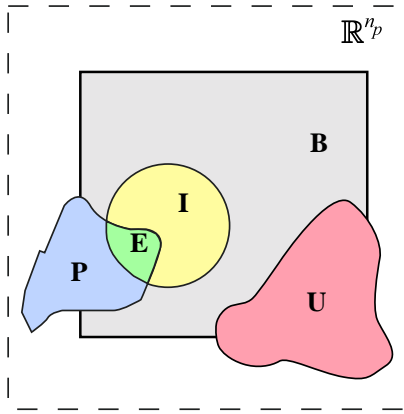


Fig. 2 Sets for problem definition.

set	description
\mathbb{R}^{n_p}	n_p -dimensional R eal valued Euclidean vector space
$\mathbf{B} \subset \mathbb{R}^{n_p}$	subset of \mathbb{R}^{n_p} , which is B ounded by (5)
$\mathbf{I} \subset \mathbf{B}$	subset of \mathbf{B} , which satisfies Isoperformance, see (3),(6)
$\mathbf{U} \subset \mathbb{R}^{n_p}$	U nstable subspace, where $\max(\text{Re}(\lambda_i)) > 0$
$\mathbf{P} \subset \mathbb{R}^{n_p}$	P areto optimal subset, satisfies (7) without constr.
$\mathbf{E} = \mathbf{I} \cap \mathbf{P}$	E fficient subset, satisfies (7) with constraints

The first task is to find the elements of the isoperformance set \mathbf{I} in \mathbf{B} . Since the performance requirements are bounded, i.e. $|J_{z,req,i}| < \infty \forall i$, it is true that the intersection $\mathbf{U} \cap \mathbf{I} = \emptyset$. In other words only stable solutions can be part of the isoperformance set, thus $\mathbf{I} \subset \overline{\mathbf{U}}$, where the overline denotes the stable, complementary set $\overline{\mathbf{U}} = \{x | x \notin \mathbf{U}\}$. The ultimate goal is to find a family of designs p_{iso}^* , which are elements of the efficient set \mathbf{E} . The efficient set is the intersection of the isoperformance set \mathbf{I} and the pareto optimal set \mathbf{P} , i.e. $\mathbf{E} = \mathbf{I} \cap \mathbf{P}$.

Previous Work

The allocation of design requirements and resources (costs) as well as an assessment of risk during early stages of a program is based on preliminary analyses using simplified models that try to capture the behavior of interest.⁶ The kernel of the **performance assessment (disturbance analysis), sensitivity and uncertainty analysis framework**, which is used as a starting point for developing the isoperformance methodology was established by Gutierrez.¹⁸ The \mathcal{H}_2 -type performances used here are defined in accordance with Zhou, Doyle and Glover.⁵⁸

The idea of holding a performance metric or value

of an objective function constant and finding the corresponding contours has been previously explored by researchers in other areas. Gilheany¹⁵ for example presented a methodology for optimally selecting dampers for multidegree of freedom systems.¹⁵ In that particular work (Fig.5) the contours of equal values of the objective function² are found as a function of the damping coefficients d_{11} and d_{22} . In the field of **isoperformance** methodology, work has been done by Kennedy, Jones and coworkers⁴⁷⁻⁴⁹ on the need within the U.S. Department of Defense to improve systems performance through better integration of men and women into military systems (human factors engineering). They present the application of isoperformance analysis in military and aerospace systems design, by trading off equipment, training variables, and user characteristics. A systematic approach to isoperformance in complex, opto-mechanical systems such as the next generation of space observatories however is lacking at this time.

A relevant field that has received a lot of attention in recent years is **integrated modeling**. This encompasses efforts to simulate complex systems in a unified and multidisciplinary environment. Important contributions to integrated modeling were made by the Jet Propulsion Laboratory (JPL) with the creation of a MATLAB based finite element package and optical modeling software called IMOS (Integrated Modeling of Optical Systems).²³ This code was developed to assist in the synthesis of initial models of optical instruments and to reduce the model creation, analysis and redesign cycle as described by Laskin and San Martin.²⁸ The IMOS package is used extensively throughout this paper for the generation and manipulation of finite element models.

The application of isoperformance to multiobjective design optimization draws on previous research results in **multidisciplinary design optimization**. A fundamental book on the theory of multiobjective optimization was published by Sawaragi, Nakayama and Tanino.⁵⁷ An important application of multiobjective optimization is concurrent control/structure optimization. Solutions of these multi-disciplinary optimizations are dependent on the type of objective functionals specified and the programming techniques employed. The method developed by Milman et al.,³⁸ does not seek the global optimal design, but rather generates a series of Pareto-optimal designs that can help identify the characteristics of better system designs. This work comes closest to the spirit followed in this paper. Masters and Crawley use Genetic Algorithms to identify member cross-sectional properties and actuator/sensor locations that minimize an opti-

²The objective function in reference¹⁵ is called ITSE = integral of time multiplied by the sum of squares of displacements and velocities of the masses.

cal performance metric of an interferometer concept.³³ A good overview of structural and multidisciplinary optimization research is given in the volume “Structural Optimization: Status and Promise” edited by Kamat,²⁵ with significant contributions by Haftka, Venkayya, Sobieszcanski-Sobieski and others.

Approach and Roadmap

A roadmap is shown in Figures 3 and 4. The flow diagram in Figure 3 comprises the **development** of the isoperformance methodology and its implementation. The dashed box comprises essentially the performance assessment and enhancement framework developed by Gutierrez.¹⁸ The analysis process starts with a given integrated model of the system of interest, which is populated by an initial design vector p^o . The performance assessment calculates the performance vector J_z^k and compares it to the requirements $J_{z,req}$. If the inequality $|\Delta J_z^k / J_z^k| < \tau$, where $\Delta J_z^k = J_z^k - J_{z,req}$, is met, we have found a solution that satisfies the isoperformance condition. We will call this solution the nominal design p_{nom} . If the relative error is larger than τ we perform a sensitivity analysis, which yields the gradient vector (Jacobian) ∇J_z^k at the k-th iteration. This is used in a gradient search algorithm, which attempts to drive all performances to the isoperformance condition by updating p^k .

Once p_{nom} is found we begin the actual isoperformance analysis. Before trying to attack the full multivariable isoperformance problem, the problem space is restricted to only two parameters $p_j, j = 1, 2$ and one performance $n_z = 1$ (Section 3). The generalization to the multivariable case with $n_p > 2$ is the topic of Section 4. The main result from the isoperformance analysis is a set of points, p_{iso} , which approximates the isoperformance set **I** in \mathbb{R}^{n_p} . If this set is empty it means that the algorithm was not able to detect elements in the isoperformance set. The recommended procedure is then to (a) switch to a more general algorithm, (b) modify the upper or lower parameter bounds p_{LB} or p_{UB} as indicated by the active constraints or (c) to modify the requirements $J_{z,req}$.

If an isoperformance solution was found the methodology proceeds to the multiobjective optimization step as described in Section 6. The solutions in the isoperformance set, p_{iso} , are evaluated for the cost objective function J_c and the risk objective function J_r . Note that a preference order can be formulated, since often multiple, possibly conflicting objectives exist. The solution is not a single “optimal” point design, but rather a family of pareto optimal designs p_{iso}^* , which make up the “efficient” set **E**. At this point a specific design vector p_{iso}^{**} has to be selected from the efficient set using engineering judgement. This design is then used for a requirements pushback analysis, which repeats a performance assessment and uncertainty analysis to

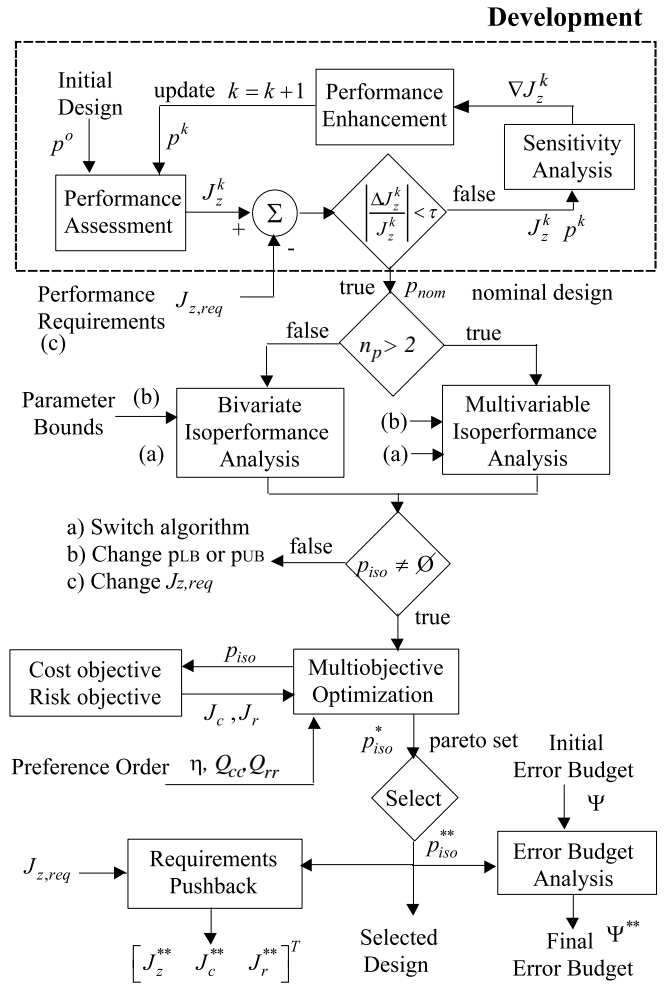


Fig. 3 Roadmap: Development

verify that indeed all performance requirements $J_{z,req}$ are met with sufficient margins, while taking into account a known or assumed uncertainty v_i of the design parameters. The resulting vectors J_z^{**}, J_c^{**} and J_r^{**} are returned giving the performance, cost and risk of the selected design.

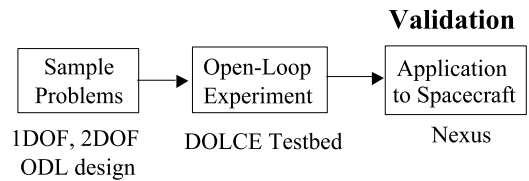


Fig. 4 Roadmap: Validation

Figure 4 contains the sequential steps used for the **validation** of the isoperformance methodology. In Section 2 we introduce a sample problem. This helps in gaining intuitive understanding and confidence in the correct implementation of the governing equations. An experimental investigation is presented in

Section 5. The experiment uses the DOLCE testbed with a uniaxial vibration exciter as the surrogate mechanical noise source. The goal of the experiment is to demonstrate the ability of the isoperformance analysis code to predict the shape and locations of isoperformance contours for combinations of system parameters such as payload mass and disturbance excitation amplitude. Once confidence has been obtained that the methodology can yield useful results on physical systems it is applied to an actual spacecraft model. The NGST precursor mission NEXUS was chosen for an in-depth analysis including performance, sensitivity, uncertainty and isoperformance analyses (Section 6). Contributions and recommendations for future work are discussed in Section 7.

2 Sample Problem

Figure 5 shows a schematic representation of the single degree-of-freedom oscillator, which is composed of a mass m [kg], a linear spring of stiffness k [N/m] and a linear damper (dashpot) with coefficient c [Ns/m]. The oscillator is excited by a zero-mean white-noise disturbance force F [N], which has been passed through a first order low-pass filter (LPF) with unity DC-gain and a corner frequency ω_d [rad/sec].

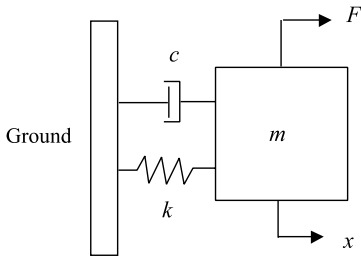


Fig. 5 Schematic of single degree-of-freedom (SDOF) oscillator.

The displacement x [m] of the mass is passed through a first order highpass filter (HPF) with corner frequency ω_o [rad/sec], simulating the effect of an optical controller. The resulting output z [m] is used to compute the performance. The performance is the RMS of z , specifically $J_z = (E[z^T z])^{1/2}$, where $E[\cdot]$ denotes the expectation operator.⁴ This system is shown in the block diagram of Figure 6.

The goal is to understand how this performance, J_z , depends on the variable design parameters, i.e. $p_i \mapsto J_z(p_i)$ for $i = 1, 2, \dots, 5$, where $p = [\omega_d \ m \ k \ c \ \omega_o]^T$. Isoperformance results for this problem are presented in the next two sections.

3 Bivariate Isoperformance Methodology

This section solves the bivariate isoperformance problem for two independent variable parameters p_j ,

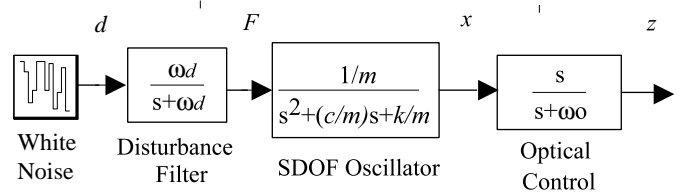


Fig. 6 SDOF block diagram. From left: white noise disturbance source, disturbance LPF, oscillator and optical control HPF.

where $j = 1, 2$, and one (scalar) performance objective $p_j \mapsto J_z(p_j)$. Three alternative algorithms (exhaustive search, gradient-based contour following and progressive spline approximation) are developed and compared. We want to find a set of solutions, p_{iso} , which satisfies the isoperformance condition (3).

Algorithm I: Exhaustive Search

This method discretizes the parameter space, defined by the upper and lower bounds $p_{j, LB}, p_{j, UB}$, where $j = 1, 2$, by overlaying a fine grid and completely evaluating all grid points. The subdivisions of the grid are defined by means of uniform parameter increments $\Delta p_1, \Delta p_2$. The size of the increments should be small enough to capture details of the isoperformance contours. This is dependent on the smoothness of $J_z(p_j)$, which is not known a priori. Small increments are desirable as this will allow to capture a large number of points p_{iso} on the isoperformance contours. On the other hand the computational expense grows significantly with smaller increments. Each grid point on the grid represents a unique parameter combination $p_{k,l} = [p_{1,k} \ p_{2,l}]^T$. The parameter values are obtained from $p_{1,k} = p_{1, LB} + (k - 1)\Delta p_1$ and $p_{2,l} = p_{2, LB} + (l - 1)\Delta p_2$, respectively, which leads to a linearly spaced grid. The performance $(J_z)_{k,l} = J_z(p_{k,l})$ is evaluated for all parameter combinations (complete enumeration). The number of increments in each parameter axis is obtained as³:

$$n_1 = \left\lceil \frac{p_{1, UB} - p_{1, LB}}{\Delta p_1} \right\rceil \quad \text{and} \quad n_2 = \left\lceil \frac{p_{2, UB} - p_{2, LB}}{\Delta p_2} \right\rceil \quad (8)$$

The index k on the first parameter runs from 1 to $n_1 + 1$, the index l runs from 1 to $n_2 + 1$ ⁴. Thus a total number of $(n_1 + 1) \times (n_2 + 1)$ combinations has to be evaluated. This is algorithmically achieved by means of two nested **for** loops. The resulting performances $(J_z)_{k,l}$ are stored in a $(n_1 + 1) \times (n_2 + 1)$ matrix. A representation of the parameter space \mathbf{B} discretization

³The $\lceil \cdot \rceil$ operator denotes the ceiling function.

⁴If $k = n_1 + 1$ then $p_{1,k} = p_{1, UB}$ and if $l = n_2 + 1$ then $p_{2,l} = p_{2, UB}$.

is shown in Figure 7.

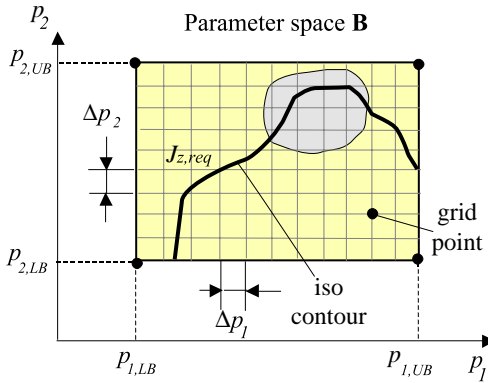


Fig. 7 Algorithm I: Discretization of \mathbf{B} in a linearly spaced grid with increments $\Delta p = [\Delta p_1, \Delta p_2]^T$.

Note that the result of a particular parameter combination $p_{k,l}$ does not affect the computation of the next point. Once all the parameter combinations $p_{k,l}$ have been evaluated, linear interpolation between neighboring grid points is used to find isoperformance points $p_{iso,r}$. The linear interpolation algorithm uses the following equation to find the r -th isoperformance point:

$$p_{iso,r} = \begin{bmatrix} p_{1,k} \\ p_{2,l} \end{bmatrix} + \frac{(J_z)_{k,l} - J_{z,req}}{(J_z)_{k,l} - (J_z)_{m,n}} \cdot \begin{bmatrix} p_{1,m} - p_{1,k} \\ p_{2,n} - p_{2,l} \end{bmatrix} \quad (9)$$

The above equation is invoked if it is found that either $(J_z)_{k,l} \geq J_{z,req} \geq (J_z)_{m,n}$ or $(J_z)_{k,l} \leq J_{z,req} \leq (J_z)_{m,n}$, assuming continuity of $J_z(p)$. This requires that the predicted performance at each grid point $(J_z)_{k,l}$ is compared to the performance of each neighboring grid point $(J_z)_{m,n}$. Note that $(J_z)_{m,n}$ is the performance at a neighboring point such that $m \in [k-1, k, k+1]$ and $n \in [l-1, l, l+1]$. The point $m = k, n = l$ is not tested, since it represents the grid point $p_{k,l}$ itself. An alternate option replaces the linear interpolation step with a call to the MATLAB built-in function `contourc.m` for contouring. This allows displaying a family of several performance levels at once.

Algorithm II: Gradient-based Contour Following

The basic idea of gradient-based contour following is to first find an ‘‘isopoint’’, $p_{iso,1}$, which is known to yield the required performance $J_{z,req}$, i.e. it lies on an isoperformance contour. Once such a point is found, a neighboring point $p_{iso,k+1}$ on the same isoperformance contour is computed by means of the gradient vector $\nabla J_z(p_1, p_2)$. Thus, a prerequisite is that $J_z(p_j)$ be continuous and differentiable at all points in the parameter space $p = [p_1, p_2]^T \in \mathbf{B}$. The desired step

direction is colinear with the tangent vector t_k to the isoperformance contour. The derivation starts by considering the bivariate function

$$p_1, p_2 \mapsto J_z(p_1, p_2), \text{ where } \mathbb{R}^2 \mapsto \mathbb{R} \text{ and } p_j \in \mathbf{B} \quad (10)$$

Next a Taylor series expansion of the vector function $J_z(p)$ is performed around a nominal point, p_{nom} , where $p_{nom} \in \mathbf{B}$, as follows:

$$J_z(p) = J_z(p_{nom}) + (\nabla J_z)^T \Big|_{p_{nom}} \cdot \Delta p + \frac{1}{2} \Delta p^T H \Big|_{p_{nom}} \Delta p + \text{H.O.T.} \quad (11)$$

Note that $p = p_{nom} + \Delta p$ and that ∇J_z and H are the gradient vector and Hessian matrix, respectively. The parameter vector increment, Δp , can be written as the product of a step size, α , and a step direction (vector), d . Note that d is normalized to unit length

$$\Delta p = \alpha \cdot d \quad (12)$$

The starting point of algorithm II is an initial guess $p_o = [p_{1,o}, p_{2,o}]^T$, which is in the ‘‘vicinity’’ of, but not necessarily exactly on the isoperformance contour. A steepest descent algorithm¹⁴ is used to obtain a first isopoint $p_{iso,1}$ on the isoperformance contour. A direction d of $J_z(p_1, p_2)$, where $\mathbb{R}^2 \mapsto \mathbb{R}$ at $p = p_o$ is a descent direction if

$$J_z(p_o + \alpha \cdot d) < J_z(p_o) \quad (13)$$

for all sufficiently small positive values of α . The step size α is a scalar value and is chosen to be positive if the initial guess p_o lies ‘‘above’’ the isoperformance contour (e.g. yields a larger J_z value). Conversely if the initial guess p_o or any subsequent iterate is ‘‘below’’ the isoperformance level, α will be a negative scalar. The next iterate is then obtained as $p_{o+1} = p_o + \alpha_o \cdot n_o$, where n_o is the unit-length vector of steepest descent. Thus, one can write the first order approximation at the point p_o as:

$$J_z(p_o + \alpha_o \cdot n_o) \cong J_z(p_o) + \nabla J_z(p_o)^T \cdot \alpha_o n_o \quad (14)$$

Recall from the Cauchy-Schwartz inequality that

$$J_z + \nabla J_z^T \left(\frac{-\nabla J_z}{\|\nabla J_z\|} \right) \leq J_z + \nabla J_z^T \left(\frac{d}{\|d\|} \right) \quad (15)$$

for any $d \neq 0$. Thus, the steepest descent vector (step direction) at p_o is obtained as

$$n_o = \left(\frac{-\nabla J_z(p_o)}{\|\nabla J_z(p_o)\|} \right) \quad (16)$$

The step size, α_o , is found by assuming linearity from the initial guess p_o to the first point on the isoperformance contour $p_{iso,1}$. From the expression

$$J_z(p_o + \alpha_o d_o) \cong J_z(p_o) + \nabla J_z^T \cdot \alpha_o n_o \equiv J_{z,req} \quad (17)$$

one can solve for α_o , such that

$$\alpha_o = \left(\frac{-\nabla J_z(p_o)^T \nabla J_z(p_o)}{\|\nabla J_z(p_o)\|} \right)^{-1} \cdot (J_{z,req} - J_z(p_o)) \quad (18)$$

This assumes that p_o is *not* an extremum or a saddle point of $J_z(p_1, p_2)$, where $\|\nabla J_z(p_o)\| = 0$ would be true. Using the above equations the algorithm generally intercepts an isoperformance contour, if it exists within \mathbf{B} , at a point $p_{iso,1}$ within a few iterations. In practice an upper limit is imposed on the step size to avoid “overshooting”, when going from a small gradient to a large gradient area of \mathbf{B} .

Given that $J_z(p_{iso,k}) = J_{z,req}$, i.e. the point $p_{iso,k}$ lies on the isoperformance contour, one can find a neighboring point $p_{iso,k+1} = p_{iso,k} + \Delta p_k$ such that $J_z(p_{iso,k} + \Delta p_k) = J_z(p_{iso,k}) = J_{z,req}$ by recalling the Taylor series expansion in (11), neglecting second-order and higher terms and setting the first order term (perturbation) to zero. Specifically, if

$$\begin{aligned} J_z(p_{iso,k+1}) &= J_z(p_{iso,k} + \Delta p_k) \cong \\ J_z(p_{iso,k}) + (\nabla J_z)^T \Big|_{p_{iso,k}} \Delta p_k &\equiv J_{z,req} \end{aligned} \quad (19)$$

is to be true, then

$$\Delta J_{z,k} = (\nabla J_z)^T \Big|_{p_{iso,k}} \Delta p_k \equiv 0 \quad (20)$$

In other words, one must choose the vector Δp_k , such that it is in the nullspace of the transposed gradient vector $(\nabla J_z)^T$. This condition can be written out componentwise as

$$\Delta J_{z,k} = \frac{\partial J_z}{\partial p_1} \Big|_{p_{1,k}} \Delta p_{1,k} + \frac{\partial J_z}{\partial p_2} \Big|_{p_{2,k}} \Delta p_{2,k} \equiv 0 \quad (21)$$

Geometrically this condition corresponds to following the tangential vector t_k along the isocontour. Figure 8 shows that t_k can be considered the tangential vector at point $p_{iso,k}$ and that it is orthogonal to the normal vector n_k . There are two ways in which t_k can be obtained from $\nabla J_z(p_k)$. First one can compute the normal vector n_k from equation (16) and then rotate it by 90 degrees to obtain the tangential vector t_k .

$$t_k = \mathcal{R} \cdot n_k = \begin{bmatrix} 0 & -1 \\ 1 & 0 \end{bmatrix} \cdot n_k \quad (22)$$

The second method is more general, since it is also applicable to the case of $n_z > 1$ performances and $n_p > 2$ parameters. A singular value decomposition (SVD)⁵⁵ is performed on the transpose of the gradient vector.

$$U_k S_k V_k^T = \nabla J_k^T \quad (23)$$

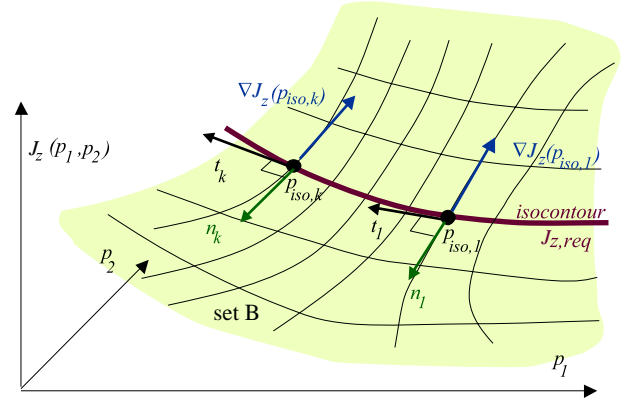


Fig. 8 Algorithm II: Depiction of gradient vector ∇J_z , normal vector n and tangential vector t along the isoperformance contour.

In the bivariate case two singular values are obtained. The non-zero singular value, $s_{1,k} \neq 0$, corresponds to the direction of steepest descent n_k and the zero singular value, $s_{2,k} = 0$, corresponds to the tangential direction t_k in matrix $V_k = [n_k \ t_k]$. An appropriate step size α_k needs to be chosen. An estimate of the linearization error incurred due to a step of size Δp_k can be written as:

$$\epsilon_k = \frac{1}{2} \Delta p_k^T H|_{p_k} \Delta p_k + \text{H.O.T.} \quad (24)$$

Neglecting higher order terms, one solves for the step size α_k , by substituting $\Delta p_k = \alpha_k \cdot t_k$ in the above equation and setting $\epsilon_k = \tau J_{z,req} / 100$.

$$\alpha_k = \left[\frac{2\tau J_{z,req}}{100} (t_k^T \cdot H|_{p_k} \cdot t_k)^{-1} \right]^{1/2} \quad (25)$$

The quantity τ is a user defined tolerance and is defined as the \pm % acceptable deviation from the nominal “centerline”, $J_{z,req}$.

With equations (22) and (25) the step direction t_k and the step size α_k have been determined and one can find the next point on the isoperformance contour $p_{iso,k+1} = p_{iso,k} + \alpha_k t_k$. At this new point the performance $J_z(p_{iso,k+1})$ is recomputed along with the gradient vector $\nabla J_z(p_{iso,k+1})$. The process is repeated until the parameter boundaries of \mathbf{B} are reached, the solution reaches the unstable subspace \mathbf{U} or the isoperformance contour closes on itself.

Algorithm III: Progressive Spline Approximation

The progressive spline approximation algorithm assumes that the isoperformance contour intersects the boundary \mathbf{B} , i.e. that no closed loops are present. This is most often the case, when the performance function $J_z(p_1, p_2)$ is monotonic in at least one of the two parameters. The basic idea of this algorithm is to approximate the isoperformance contour with a piecewise

polynomial (pp) function. The spline mathematics and tools developed by de Boor⁷ as well as the resulting MATLAB spline toolbox are leveraged for this algorithm.

A mathematical description of a spline, $P_l(x)$, is given in terms of its break points (**breaks**) $\zeta_1, \dots, \zeta_{l+1}$ and the local polynomial coefficients $c_{l,i}$ of its **pieces**.

$$P_l(x) = \sum_{i=1}^k \frac{(x - \zeta_j)^{k-i}}{(k-i)!} c_{l,i} \quad (26)$$

This form (**ppform**) is especially convenient for evaluation, while the **B-form** is often used for construction of a spline approximation. The **order** is chosen as $k = 4$, which leads to cubic splines and two continuous derivatives across the break points. The progressive spline approximation algorithm assumes that the two endpoints a, b are on the parameter space boundary **B**. The initial estimate of the isoperformance contour consists of a single piece. The isoperformance contours are parameterized with parameter t from endpoint a to endpoint b we set $t = 1.0$. Instead of the coordinates x and $y = f(x)$ as in Equation (26) the algorithm works with *vector* splines such that

$$P_l(t) = \begin{bmatrix} p_{iso,1}(t) \\ p_{iso,2}(t) \end{bmatrix} = \begin{bmatrix} s_1(t) \\ s_2(t) \end{bmatrix} = p_{iso}(t) \quad (27)$$

where

$$t \in [0, 1] \mapsto P_l(t) \in [a, b] \quad (28)$$

the vector components of each spline **piece** are approximated as piecewise polynomials in **ppform**, where

$$s_j(t) = f_{j,l}(t) \text{ for } j = 1, 2 \text{ and } \forall l \quad (29)$$

The functional approximation for each piece is then given as

$$f_{j,l}(t) = \sum_{i=1}^k \frac{(t - \zeta_l)^{k-i}}{(k-i)!} c_{j,l,i} \text{ where } t \in [\zeta_l \dots \zeta_{l+1}] \quad (30)$$

Note that *all* relevant information is contained in the break point sequence, $\zeta_1 \dots \zeta_{l+1}$ and in the polynomial coefficient array $c_{j,l,i}$. The subscript j refers to the vector component of p_{iso} , l refers to the piece number of the **pp** approximation and i is the index of the polynomial degree. In practice the coefficient array $c_{j,l,i}$ is stored as a 2-dimensional matrix by stacking the coefficient matrices of the vector components j on top of each other, along the first non-singleton dimension.

Next a bisection is performed at the mid-point of the first piece, ($t = 0.5$), resulting in the point $p_{mid,1}$. If the true isoperformance contour is close to the cubic spline approximation, then $p_{mid,1}$ will lie on the contour. Generally this will not be the case and $p_{mid,1}$

is then used as the starting point for a steepest gradient search to find the closest point on the contour. This point $p_{iso,1}$ represents a new break ζ_2 and splits the original interval $[a, b]$ into two pieces. The MATLAB function `csape.m` is used to compute the spline coefficient matrix c for the pieces $[a = \zeta_1, \zeta_2]$ and $[\zeta_2, b = \zeta_3]$. This bisection procedure is repeated until the midpoints of all pieces lie on the contour, subject to a tolerance τ as defined above. This is graphically shown in Figure 9 for the single degree-of-freedom example introduced in Section 2.

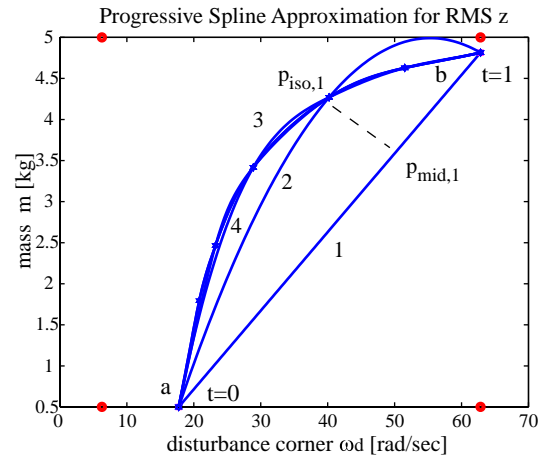


Fig. 9 Progressive (cubic) spline approximation. Isoperformance analysis of SDOF problem with variables ω_d and m . The required performance is $J_{z,req} = 0.0008$ [m].

Algorithm Evaluation

This section applies the three algorithms, which have been implemented in MATLAB code, to the single DOF sample problem and quantitatively as well as qualitatively compares the answers. The conclusions provide guidance for applications to larger problems and the multivariable case. We choose the disturbance corner frequency, ω_d , and oscillator mass, m , as the variable parameters in order to find the isoperformance contour at the $J_z = 0.8$ [mm] level.

Quality of Isoperformance Solution

In order to assess how well the resulting isoperformance points, p_{iso} , actually meet the isoperformance condition (3) it is necessary to define a solution “quality” metric. The “quality” of the isoperformance solution can be quantified as follows. Let

$$\Upsilon_{iso} = \frac{100}{J_{z,req}} \cdot \left[\frac{\sum_{k=1}^{n_{iso}} [J_z(p_{iso,k}) - J_{z,req}]^2}{n_{iso}} \right]^{1/2} \quad (31)$$

be a quality metric expressing the relative % error

with respect to $J_{z,req}$. In the above equation n_{iso} is the total number of isopoints computed, $J_z(p_{iso,k})$, is the performance of the k-th isopoint and $J_{z,req}$ is the performance requirement, i.e. the desired performance level. This number, Υ_{iso} , can then be directly compared to the desired isoperformance contour tolerance, τ , and should always be smaller than it. Note that this definition of solution quality does not prevent individual solutions p_{iso} from falling outside the tolerance band $[(1 - \tau/100) \cdot J_{z,req}, (1 + \tau/100) \cdot J_{z,req}]$.

Algorithm Comparison

The isoperformance results for exhaustive search are shown in Figure 10. The isoperformance curve shows that a small increase in the disturbance filter corner frequency ω_d below about 30 radians per second (roughly 5 Hz), which is the natural undamped frequency of the oscillator, requires a large increase in mass m in order to maintain the same RMS level.

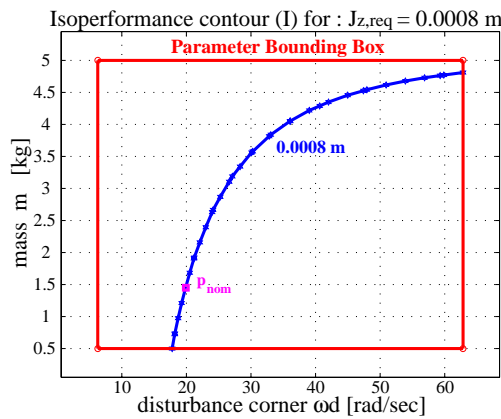


Fig. 10 Algorithm I (Exhaustive Search): Isoperformance contour for single DOF problem (ω_d, m) with discretization $\Delta p = (1/20)[p_{UB} - p_{LB}]$ and a tolerance of $\tau = 1\%$.

The quality of the isoperformance contour is very dependent on the discretization level. The smaller Δp , the better the contour will be interpolated but the more computation time is required. For the exhaustive search algorithm the solution quality is shown in Figure 11.

The isoperformance contours obtained with contour following (not shown) and progressive spline approximation (Fig. 9) are very similar. A comparison of the computational cost among algorithms is shown in Table 1. In order to achieve a fair comparison it was deemed necessary that all three methods yield isoperformance solutions of nearly equal quality as expressed by the Υ_{iso} metric. Algorithm I is the most computationally expensive. This is due to the fact that in the SDOF case 441 points had to be evaluated, but only 35 points form the isoperformance contour. Algorithm III (progressive spline approximation) is clearly the fastest, however it only works for open segments

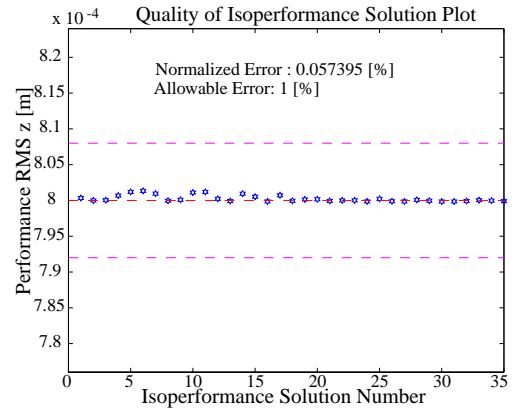


Fig. 11 Quality: Contour solution quality according to (31).

Table 1 Comparison of algorithms I-III for single DOF problem.

Result	Ex Search	Co Follow	Sp Approx
FLOPS	2,140,897	783,761	377,196
CPU [sec]	1.15	0.55	0.33
Tolerance: τ	1.0 %	1.0 %	1.0 %
Error: Υ_{iso}	0.057 %	0.379 %	0.087 %
isopoints	35	41	7

and assumes that there is only a single isoperformance contour, which intersects the boundary **B**. Thus, it is the most restrictive (least general) of the three algorithms. The second algorithm (gradient-based contour following) has a computational cost which is in between the other two methods. Multiple open or closed segments can be detected, but several random trial points $p_{nom,i}$, where $i = 1, 2, \dots, \#$ of trial points, are required to detect multiple contours. The advantage of this method is that it uses knowledge about the previous points, $p_{iso,k}$, obtained in order to compute the next isoperformance solution $p_{iso,k+1}$. Another advantage is that the step size, α_k , automatically adjusts according to the local curvature of $J_z(p_{iso,k})$ by means of a finite difference approximation of the Hessian matrix. The disadvantage of algorithm II is that one must recompute the gradient $\nabla J_z(p_{iso,k})$ at each new isopoint. The generalization of these algorithms to the multivariable case is discussed in the next section.

4 Multivariable Isoperformance Methodology

This section generalizes the algorithms developed in the previous section to the multivariable case. This generalization is essential in order to render isoperformance a useful technique for realistic problems. Specifically, there can be more than two variable pa-

rameters and multiple performances, i.e. $n_p > 2$ and $n_z > 1$. The condition that the number of variable parameters always exceeds the number of performances $n_p - n_z > 1$ has to be maintained in order for there to be a non-zero isoperformance set. There are two main challenges in the multivariable case:

- Complexity as a function of n_p and n_z
- Visualization of isoperformance set \mathbf{I} in \mathbb{R}_p^n

Branch and Bound Search Algorithm (Ib)

The exhaustive search algorithm (Ia) in the multivariable case ($n_p > 2$) discretizes the parameter set \mathbf{B} , defined by the lower and upper bounds $p_{LB,j}$ and $p_{UB,j}$, where $j = 1, 2, \dots, n_p$, with a fine grid and evaluates all grid points. This was presented for the case, when $n_p = 2$ in Section 3. Subsequently each grid point is tested, and if the isoperformance condition (6) is met, the grid point is retained in the isoperformance set \mathbf{I} . The exhaustive search algorithm for the multivariable problem can be implemented as n_p -nested loops. Note that the value of the j -th parameter in these loops is given as

$$p_{j,i_j} = p_{j,LB} + (i_j - 1) \cdot \Delta p_j \quad \text{where} \quad j = 1, 2, \dots, n_p \quad (32)$$

Clearly, this is not practical even for relatively modest problems. Assume for example that $n_p = 6$ and that $n_1 = \dots = n_{n_p} = 50$, then the performance evaluation $p_j \mapsto J_z$ has to be carried out $50^6 = 1.56 \cdot 10^{10}$ times. If it took one second of CPU time per performance evaluation it would take 495.5 years to evaluate the entire trade space on a single computer.

A remedy is found by modifying exhaustive search as a branch-and-bound algorithm (Ia). The branch-and-bound algorithm starts with an initial population (branches), which are evenly but coarsely distributed in \mathbf{B} . It then tests if the performance at neighboring points (branches), p_m and p_n , is such that the isoperformance surface passes in between them:

$$[J_z(p_m) \geq J_{z,req} \geq J_z(p_n)] \cup [J_z(p_m) \leq J_{z,req} \leq J_z(p_n)] \quad (33)$$

where p_m, p_n are $n_p \times 1$ vectors and $J_{z,req}$ is a $n_z \times 1$ vector. If the answer is **true**, both branches are retained and further refined in the next generation. If the answer is **false** the point (branch) p_m is eliminated. This is graphically shown in Figure 12 for two dimensions.

In the multivariable case the squares shown in Figure 12 are actually hyper-rectangles. The size of the hyper-rectangles is reduced by a factor of two along edges with each generation. This refinement continues with each generation, n_g , until the exit criterion

$$\Upsilon_{iso,n_g} < \tau \quad (34)$$

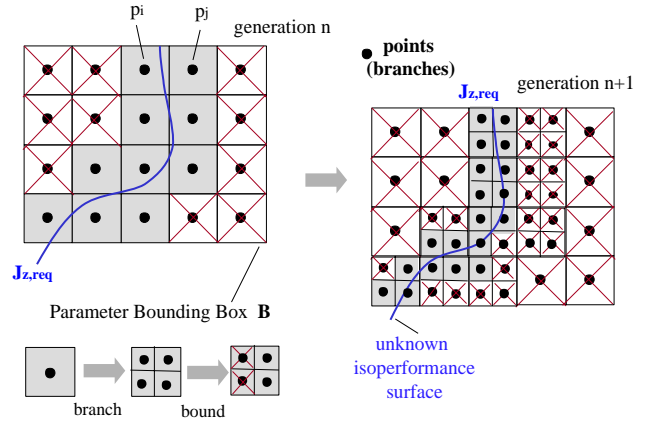


Fig. 12 Multivariable Isoperformance (Ib): Branch-and-Bound graphic representation. Crossed out points (branches) are dropped in the next generation.

is met.

It was empirically found that setting a tolerance tighter than 2% becomes very expensive, since in the branch and bound approach each generation is roughly 2^{n_p} times larger than the previous generation. An advantage of the branch-and-bound algorithm, however, is that it does not require any sensitivity (gradient) information.

Tangential Front Following Algorithm

In the multivariable case there will be n_z performance metrics and n_p parameters, where $n_p - n_z \geq 1$. A first order Taylor approximation of the vector performance function J_z at a point $p^k = [p_1^k \ p_2^k \ \dots \ p_{n_p}^k]^T \in \mathbf{B}$ can be written as:

$$J_z(p^{k+1}) = J_z(p^k + \Delta p) = J_z(p^k) + \nabla J_z^T|_{p^k} \Delta p + \text{HOT} \quad (35)$$

The Jacobian, ∇J_z , is the matrix of first order partial derivatives of J_z with respect to p :

$$\nabla J_z = \begin{bmatrix} \frac{\partial J_{z,1}}{\partial p_1} & \frac{\partial J_{z,1}}{\partial p_2} & \dots & \frac{\partial J_{z,1}}{\partial p_{n_p}} \\ \frac{\partial J_{z,2}}{\partial p_1} & \frac{\partial J_{z,2}}{\partial p_2} & \dots & \frac{\partial J_{z,2}}{\partial p_{n_p}} \\ \vdots & \vdots & \ddots & \vdots \\ \frac{\partial J_{z,n_z}}{\partial p_1} & \frac{\partial J_{z,n_z}}{\partial p_2} & \dots & \frac{\partial J_{z,n_z}}{\partial p_{n_p}} \end{bmatrix} \quad (36)$$

The singular value decomposition (SVD) of the Jacobian is a key step. It provides a set of orthogonal unit-length vectors, v_j , as the columns of matrix, V , thus forming the column space and null space of the Jacobian, respectively.

$$U \Sigma V^T = \nabla J_z^T \quad (37)$$

and the individual matrices are as follows:

$$\begin{aligned}
 U &= \begin{bmatrix} u_1 & \cdots & u_{n_z} \end{bmatrix} \\
 \Sigma &= \begin{bmatrix} \text{diag}(\sigma_1 \cdots \sigma_{n_z}) & 0_{n_z \times (n_p - n_z)} \\ \hline & \end{bmatrix} \\
 &\quad \underbrace{\hspace{10em}}_{n_z \times n_p} \quad (38) \\
 V &= \begin{bmatrix} v_1 & \cdots & v_{n_z} & v_{n_z+1} & \cdots & v_{n_p} \\ \hline \text{column space} & & \text{null space} & & & \end{bmatrix}
 \end{aligned}$$

Thus, at each point there are $n_p - n_z$ directions in the null space. It is a linear combination of the vectors in the null space, V_t , which is used to determine a tangential step, Δp , in a performance invariant direction.

$$\Delta p = \alpha \cdot (\beta_1 v_{n_z+1} + \cdots + \beta_{n_p - n_z} v_{n_p}) = \alpha V_t \beta \quad (39)$$

where Δp is the performance invariant step increment in \mathbb{R}^{n_p} , β is a vector of coefficients, which determines the linear combination of directions in the nullspace, V_t , and α is a step size. Currently, in the multivariable case the step size, α , is set by the user. An automatic step size determination could be added as a refinement in the future. The coefficient vector, β , is determined as follows

$$\beta = \begin{cases} \beta_i = \pm 1, \beta_j = 0 \text{ for } i \neq j \\ \beta_i = \pm \frac{1}{\sqrt{n_p - n_z}} \quad \forall \quad i = 1, \dots, n_p - n_z \end{cases} \quad (40)$$

The principal front points, as shown in Figure 13, propagate in one of the positive or negative directions given by the principal vectors, v_i , in the null space. The intermediate front points on the other hand propagate in directions, which have equal contributions from all vectors in v_t . The \pm sign for each β_i determines in which ‘‘quadrant’’ the front point propagates.

The tangential front following algorithm is a generalization of the gradient-based contour following algorithm, which was developed for the case when $n_p - n_z = 1$, see subsection 3. *The idea is to gradually explore the isoperformance set \mathbf{I} , starting from a random initial point, p_{nom} , and subsequently stepping in tangential, orthogonal directions, v_j , where $j = n_z + 1, \dots, n_p$, which lie in the null space of the Jacobian.* The active points form a ‘‘front’’, when connected to each other. The front grows gradually outwards from the initial point until the boundary is intercepted. This is similar to ‘‘moss’’, which grows from an initial seed to gradually cover the entire exposed surface of an imaginary n_p -dimensional rock. This is shown graphically in Figure 13.

The main advantage of this algorithm, is that it converts the computational complexity from a n_p to a $n_p - n_z$ problem, albeit still in non-polynomial time. The disadvantage of the algorithm is that a

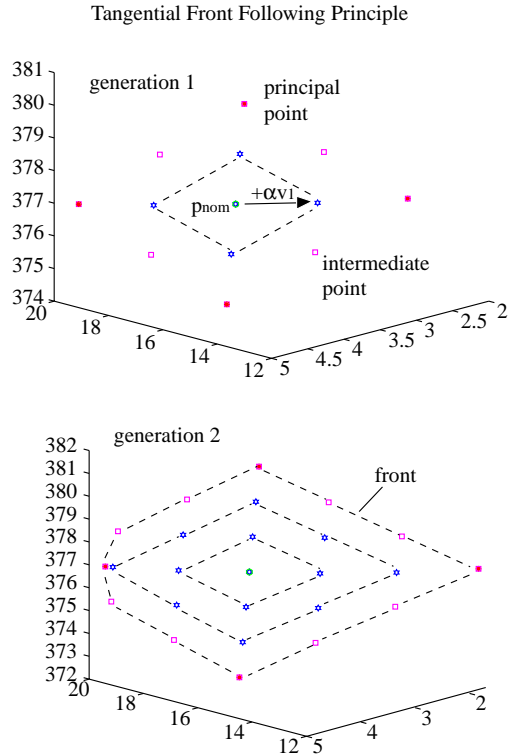


Fig. 13 Tangential Front Following (II) principle.

non-uniform distribution of isoperformance points can result from the behavior of the Jacobian in different regions of the set \mathbf{B} or at the boundary of \mathbf{B} . The underlying performance function $J_z(p)$ has to be continuous and differentiable over the entire set \mathbf{B} .

Vector Spline Approximation

Even though the tangential front following algorithm is more efficient than branch-and-bound, it will still be computationally expensive if $n_p - n_z$ is large. An estimate of the computational expense of each algorithm is given below. Hence, it is desirable to find an algorithm with a further significant increase in efficiency. Such an algorithm is constructed by generalizing the bivariate progressive spline approximation. *The basic idea of vector spline approximation is to only capture important border and interior points of the isoperformance set \mathbf{I} .* A t -parameterized vector spline in n_p -dimensional space connecting two points A and B can be written as

$$p(t) = \begin{bmatrix} p_1(t) \\ p_j(t) \\ \vdots \\ p_{n_p}(t) \end{bmatrix} = \begin{bmatrix} \sum_{i=1}^k \frac{(t-t_A)^{k-i}}{(k-i)!} \cdot c_{1,i} \\ \sum_{i=1}^k \frac{(t-t_A)^{k-i}}{(k-i)!} \cdot c_{j,i} \\ \vdots \\ \sum_{i=1}^k \frac{(t-t_A)^{k-i}}{(k-i)!} \cdot c_{n_p,i} \end{bmatrix} = C \cdot \hat{t} \quad (41)$$

where C is the vector spline coefficient matrix and \hat{t} is a vector, which depends on the parameter t

$$\hat{t} = \left[1 \quad \cdots \quad \frac{(t-t_A)^{k-i}}{(k-i)!} \quad \cdots \quad \frac{(t-t_A)^{k-1}}{(k-1)!} \right]^T \quad (42)$$

whereby $t \in [t_A, t_B]$ if the spline connects the points A and B in n_p -space. The vector spline approximation algorithm uses cubic splines of order, $k = 4$, one can then write:

$$\hat{t}(t) = \left[1 \quad t-t_A \quad \frac{(t-t_A)^2}{2} \quad \frac{(t-t_A)^3}{6} \right]^T \quad (43)$$

and the cubic spline coefficient matrix, C , simplifies to

$$C = \begin{bmatrix} c_{1,1} & c_{1,2} & c_{1,3} & c_{1,4} \\ \vdots & \vdots & \vdots & \vdots \\ c_{j,1} & c_{j,2} & c_{j,3} & c_{j,4} \\ \vdots & \vdots & \vdots & \vdots \\ c_{n_p,1} & c_{n_p,2} & c_{n_p,3} & c_{n_p,4} \end{bmatrix} \quad (44)$$

The first step of the vector spline approximation algorithm is to find the border points, $p_{iso,border}$, which meet the isoperformance condition (3) and lie on an edge of the parameter bounding box \mathbf{B} . These points are found by first computing the performance vector, J_z , at all 2^{n_p} corner points and searching for boundary points, $p_{iso,border}$, which lie on an edge connecting two corner points, which meet the condition

$$\begin{aligned} J_z(p_{corner,i}) &\leq J_{z,req} \leq J_z(p_{corner,j}) \cup \\ J_z(p_{corner,i}) &\geq J_{z,req} \geq J_z(p_{corner,j}) \end{aligned} \quad (45)$$

The next step is to connect the isoperformance border points with cubic splines along the boundary of \mathbf{B} . In this step the mid-points of the border splines are also determined. Finally interior points of the isoperformance set \mathbf{I} are obtained by computing the *centroid*. This can be considered to be the center point of \mathbf{I} . An initial guess for the centroid is:

$$\begin{aligned} \hat{p}_{cent} &= \left[\hat{p}_{c,1} \quad \cdots \quad \hat{p}_{c,j} \quad \cdots \quad \hat{p}_{c,n_p} \right]^T \\ \text{where } \hat{p}_{c,j} &= \frac{1}{n_b} \sum_{i=1}^{n_b} p_{iso,border,i,j} \end{aligned} \quad (46)$$

and n_b is the number of border points. The actual centroid, p_{cent} , is found by steepest gradient search as described before. Finally the cubic splines connecting the centroid and the mid-points of the border splines are found, subject to tolerance, τ .

The vector spline approximation algorithm does not provide the same large number of isoperformance points, p_{iso} , and “continuous” approximation to \mathbf{I}

as branch-and-bound or tangential front following. Rather, it only computes some key points and their connecting splines. This might be acceptable, since one of the goals of the isoperformance methodology is to find solutions which are very “different” in a design vector sense, while still yielding the same performance vector J_z .

The multivariable SDOF problem was tackled by the vector spline approximation algorithm. The three variable (design) parameters, ω_d , m and ω_o are considered. The desired performance level is $J_{z,req} = 0.8$ [mm] RMS. Results for the single DOF oscillator problem are shown in Figure 14. The outline of the isoperformance surface can clearly be seen.

Multivariable Isoperformance (III): Vector Spline Approximation

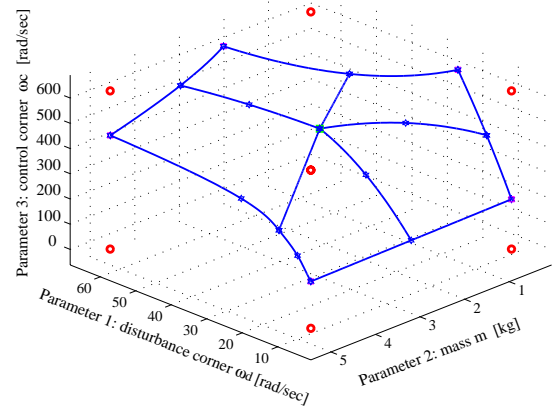


Fig. 14 Multivariable Isoperformance (III): Vector Spline Approximation for SDOF sample problem.

Multivariable Algorithm Comparison

A comparison of the multivariable algorithms using the single degree-of-freedom problem is presented in Table 2. The algorithms are compared based on the CPU runtime, the number of floating-point operations required, the solution quality expressed as Υ_{iso} and the number (quantity) of isoperformance points, p_{iso} , found.

Even though the above numbers are obtained for a specific low-order example, the relative trends between algorithms are likely to apply to large-order problems as well. As expected the exhaustive search is the most expensive algorithm and requires almost 1.5 hours to run. The vector spline approximation on the other hand completes in merely 5 seconds. Branch-and-Bound improves over exhaustive search by a factor of roughly 10 and tangential front following in turn improves over branch-and-bound by a factor of roughly 7. The tangential front following algorithm results in the best numerical solution quality as measured by, Υ_{iso} . Branch-and-Bound provides the largest number of isopoints (~ 7500), whereas vector spline approximation yields “only” 20 such points. Recall, however,

Table 2 Comparison of multivariable algorithms for SDOF problem: (Ia) Exhaustive Search, (Ib) Branch-and-Bound, (II) Tangential Front Following and (III) Vector Spline Approximation.

Metric	Ia	Ib	II	III
MFLOPS	6,164	891	106	1.5
CPU time [s]	5078	498	69	4.5
Tolerance τ	1.5 %	2.5 %	1.5 %	1.5%
Error Υ_{iso}	0.87 %	2.43 %	0.22 %	0.42 %
# of isopoints	2073	7421	4999	20

that the spline approximation also provides the spline coefficient matrices, such that additional points could be easily generated along the connecting splines.

Vector spline approximation is the most restrictive algorithm in the sense that it requires the underlying performance vector function, $p_j \mapsto J_z(p_j)$, where $p_j = 1, \dots, n_p$, to be continuous, smooth, differentiable and quasi-monotonic in \mathbf{B} . Thus, if \mathbf{I} were a closed region with no boundary points on \mathbf{B} , the vector spline approximation would fail. Tangential front following does not require quasi-monotony and can deal with closed regions. Here the problem is that if \mathbf{I} consists of several, distinct regions in \mathbf{B} the algorithm requires several random initial guesses, p_o , in order to find all regions. There is no guarantee of completeness with a finite number of trial points. Distinct regions are rarely observed in practice.

Finally branch-and-bound is the most general algorithm and is very robust, as long as the initial grid is chosen reasonably fine. Another advantage of branch and bound is that it does not require gradient (sensitivity) information. The general strategy is to first attempt an isoperformance solution with vector spline approximation and move to the other, more expensive algorithms if a solution in \mathbf{B} is expected to exist but cannot be found. This algorithm switching strategy was suggested in the paper roadmap, see Figure 3.

5 Experimental Validation

The goal of the experimental validation is to demonstrate the ability of the isoperformance methodology to accurately predict performance contours for a physical laboratory testbed in a 1g environment.

Testbed Description

The DOLCE testbed shown in Figure 15 was explicitly designed for this purpose. The main feature of DOLCE is that system parameters can be varied over a large range. This is different from the cantilever truss employed by Gutierrez,¹⁸ which was used for physical parameter sensitivity validation via small

perturbations of masses and stiffnesses. The four variable parameters on DOLCE are:

- V_s excitation RMS voltage [V]
- m_p payload mass [lbs]
- m_s seismic mass [g]
- k_s suspension spring stiffness [lbs/in]

Figure 15 shows the testbed, which, starting from the top, is comprised of an uniaxial vibration exciter (shaker), with a seismic mass, m_s , driven by a band-pass filtered (0-100 Hz), random excitation voltage, V_s . Next the upper stage contains a single small bay of a square truss and a coupling plate. The lower stage consists of a large square truss, a weight bed holding a payload mass, m_p , and an aluminum sandwich base plate. Finally an axial stabilization system and four (4) suspension springs of stiffness k_s complete the arrangement.

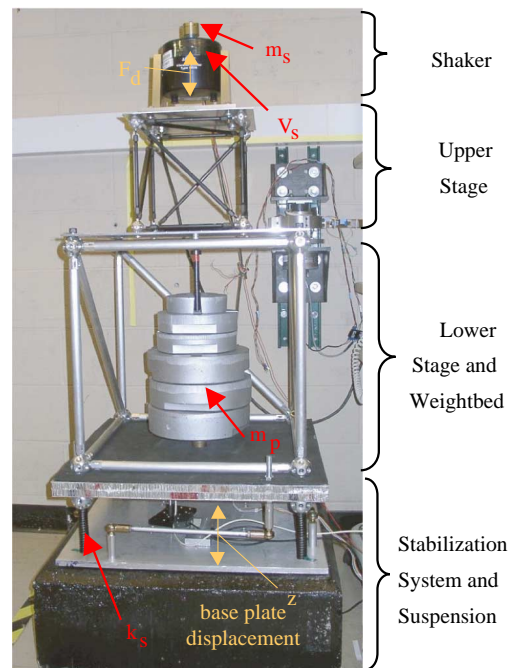


Fig. 15 DOLCE Testbed

The shaker generates a random axial disturbance force, F_d , whose magnitude and frequency content depend on the excitation voltage, V_s , and the seismic mass, m_s . This device is meant to simulate the disturbances generated by vibrating on-board machinery on a spacecraft (e.g. reaction wheel, cryocooler), albeit at a significantly higher force level. The performance is the root-mean-square (RMS) of the base plate displacement

$$J_z = E [z^T z]^{1/2} \quad (47)$$

This would correspond to jitter of the spacecraft bus in a real space system. The primary instrumentation consists of a uniaxial load cell, which is attached to the seismic mass and measures the disturbance force, F_d . The performance is measured via an inductive proximity, which acts as a gap sensor (eddy current gap sensor Bentley XL 5mm). The gap sensor is very sensitive and was calibrated to 0.425 V/mil of displacement with a LB-11/70 Laser Displacement Sensor. Also a Sunstrand DC accelerometer was installed in order to corroborate the gap sensor results. The sensor suite below the sandwich plate is shown in Figure 16.

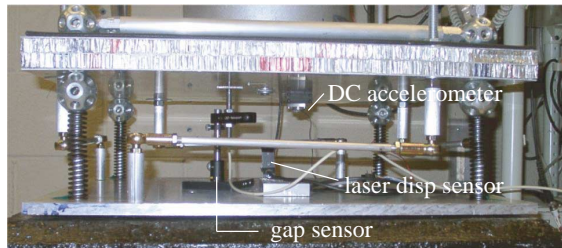


Fig. 16 DOLCE Testbed Sensors

Experimental Approach

The experimental approach is presented in Figure 17. First the testbed was assembled, instrumented and calibrated. It was decided to conduct a bivariate isoperformance test, with the performance given by Equation 47. The variable parameters were the excitation voltage, V_s , ranging from 0.1-1.0 [Vrms] as well as the payload mass, m_p , ranging from 0-200 [lbs]. A test matrix was run on the testbed and recorded with parameter increments $\Delta V_s = 0.1$ and $\Delta m_p = 10$, respectively. From this gridded data isoperformance contours were extracted via linear interpolation, see above.

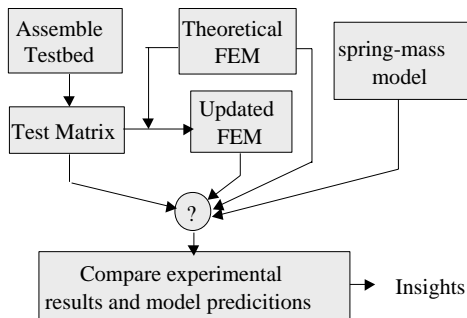


Fig. 17 Experimental Approach

Independently and without knowledge of the experimental results an a priori finite element model (FEM) was constructed (“original FEM”). This model only used assembly drawings, masses from scale measurements and catalogue values for material properties and spring stiffnesses. The predictions from this model would be equivalent to what could be expected from

isoperformance analyses for spacecraft in the conceptual and preliminary design phases, such as NEXUS. A more accurate prediction is expected from an updated FEM, which has its physical parameters tuned such that the FEM and experimental transfer function (measurement model) from F_d to z coincide well. Finally the isoperformance contours for DOLCE are predicted with a single degree-of-freedom (SDOF) model, which lumps the entire testbed mass together with the payload mass m_p over the four suspension springs (in parallel) represented as a single compliance. The hope is that insights can be gained by comparing different performance contours for the experiment with the ones predicted for the three models.

Testbed Characterization

The transfer function (FRF) from disturbance (shaker) force to base plate displacement, $G_{zd}(s) = Z(s)/F_d(s)$, where $s = j\omega$, is obtained experimentally and by model prediction, see Figure 18.

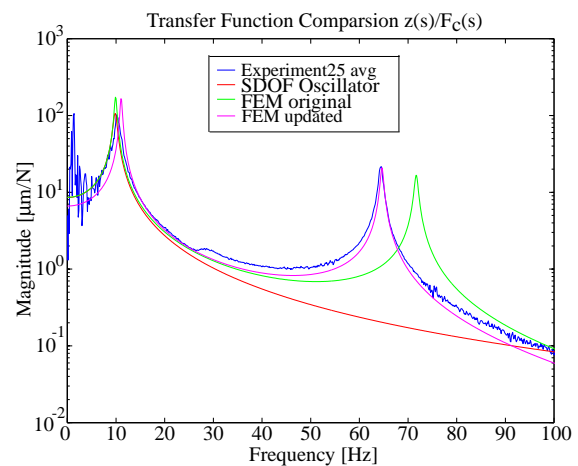


Fig. 18 DOLCE transfer function $G_{zd} = Z(s)/F_d(s)$ for $m_p = 0$, $V_s = 1.0$

As can be seen there are two observable modes in the bandwidth up to 100 Hz. The first mode at 10 Hz is the axial base suspension mode, where the testbed translated vertically up and down on the 4 suspension (compression) springs. The second mode at 65 Hz is the upper coupling plate bending mode, which causes a vertical displacement via the center rod. Mode shapes for these two modes are contained in Figure 19.

As expected the SDOF model can only predict the first resonance. The original FEM overpredicts the upper plate mode by roughly 10 Hz. The agreement between the updated FEM and the experimental transfer function is very good.

Next the testbed response was investigated as a function of the single parameter m_p . A waterfall plot showing the power spectral density (PSD) of z as a function of m_p is depicted in Figure 20.

It can be seen that the axial suspension mode is

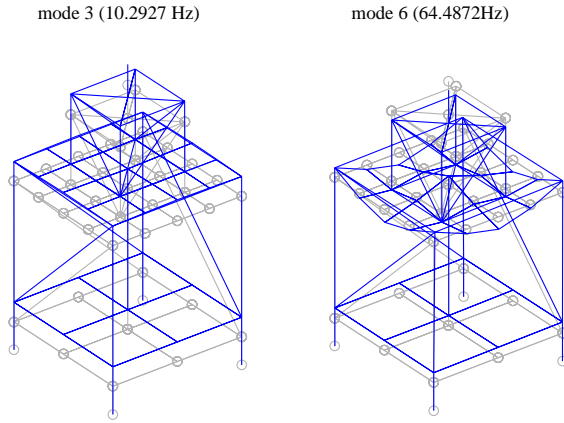


Fig. 19 DOLCE Testbed Observable Modes

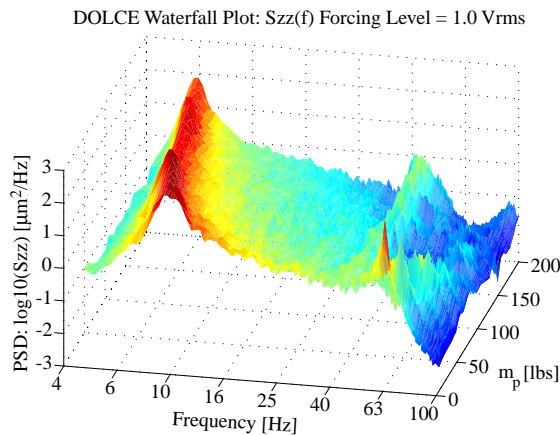


Fig. 20 Waterfall Plot for 1.0 Vrms forcing level

dominant for all payload masses. As expected the mode softens with increasing mass from about 10 Hz at $m_p = 0$ [lbs] to 6 Hz at $m_p = 200$ [lbs]. The resonant plate mode at 65 Hz can also be seen, but it is much less clear for larger m_p . A higher frequency mode around 40Hz appears m_p -invariant and we suspect some structural non-linearity. The performance J_z can be computed by integrating under S_{zz} and taking the square root.

$$J_z = \left[2 \int_{f_{min}}^{f_{max}} S_{zz}(f) df \right]^{1/2} \quad (48)$$

Isoperformance Results and Interpretation

The basis for obtaining the experimental isoperformance contours is the test matrix with V_s and m_p as described previously. At each parameter combination the time histories of $F_d(t)$ and $z(t)$, were recorded and the performance $J_z = J_z(V_s, m_p)$ was computed with 25 averages. The results from the test matrix are shown in Figure 21.

The peak displacement RMS value of 57.6 μm is obtained for the maximum excitation level ($V_s = 1.0$

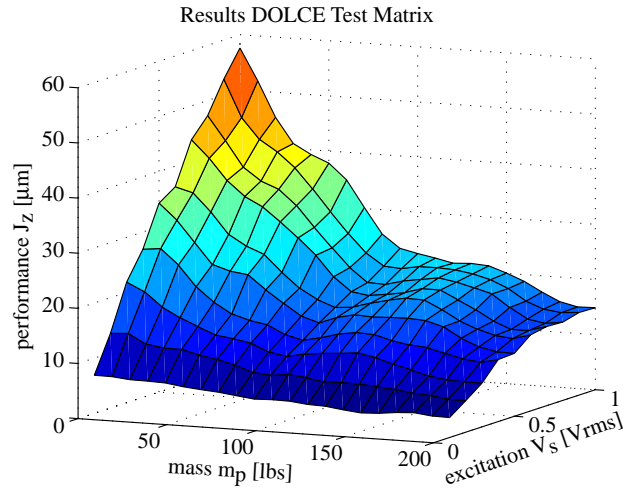


Fig. 21 DOLCE Test Matrix

[Vrms]) with an empty weight bed ($m_p = 0$ [lbs]). This is intuitively satisfactory, since at this point the maximum disturbance energy enters the system (about 7 N of force F_d RMS), while the disturbability of the system is at a maximum. Recall that the plant transfer function for such a system has a $1/m$ term in the numerator. Conversely the lowest response (“best performance”) is found for $V_s = 0.1$ and $m_p = 200$. This information is used to obtain isoperformance contours at the 7.5, 15 and 30 μm levels (Figure 22).

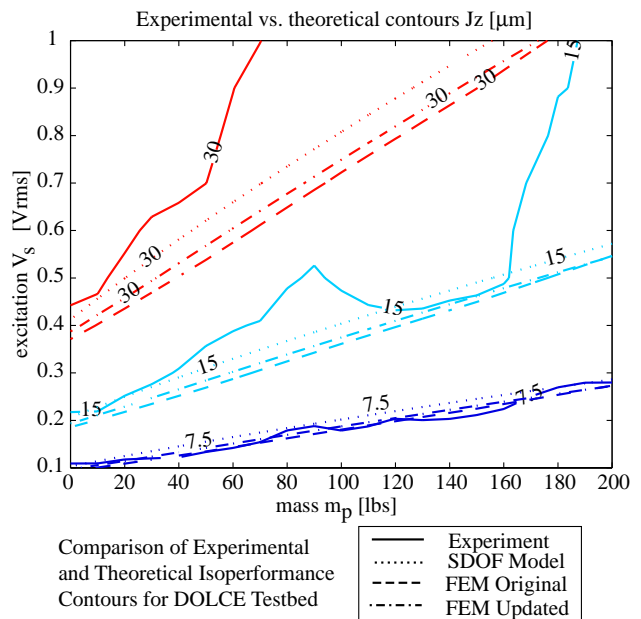


Fig. 22 DOLCE Testbed Comparison of Experimental versus Theoretical Isoperformance Contours

Similar contours are predicted for the SDOF and FEM’s (original and updated). This suggests that the axial suspension mode is dominant in most of the trade space. Excellent correlation between experiment and

theory is found at low forcing levels, see the $7.5 \mu\text{m}$ contour. Deviations are found for larger forcing levels (15 and $30 \mu\text{m}$ contours), even though the general trends are still predicted correctly by the isoperformance models. The cause for this deviation is likely due to non-linear effects in the structural plant as the shaker amplitude increases. In conclusion it is found that the isoperformance prediction capability is good at low disturbance levels which are representative of the vibration environment on space based opto-mechanical systems. Caution must be exercised if non-linearities are suspected in any part of the system.

6 NEXUS Spacecraft Study

At this point confidence has been gained that the isoperformance methodology is applicable to large order multivariable systems and that isoperformance predictions for real physical systems are possible. The purpose of the NEXUS spacecraft case study is to demonstrate the usefulness of the isoperformance methodology on a realistic conceptual design model of a high-performance spacecraft.

NEXUS Description

A graphical representation of the launch and on-orbit configurations of NEXUS is shown in Figure 23.

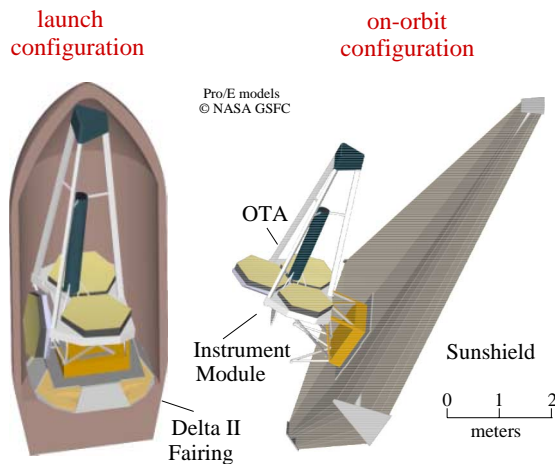


Fig. 23 NEXUS Spacecraft Concept

NEXUS was planned as a technology risk-reduction experiment in space and as a precursor to NGST. The NEXUS project was officially canceled in December 2000 as a part of the NGST rescoping exercise. It was nevertheless decided to use NEXUS for this case study, since the conceptual model is well developed and many lessons learned from previous NGST Yardstick models were incorporated.

NEXUS features a 2.8 m diameter primary mirror, consisting of three AMSD-sized primary mirror (PM) petals. Two of these are fixed and one is deployable as shown in Figure 23 on the left side. The

total mass of the spacecraft is nominally 752.8 [kg] at a cost of \$M 105.88 (FY00). The target orbit is L2 of the Sun/Earth system with a projected launch date of 2004. The optical telescope assembly (OTA) also features a 3-legged spider, which supports the secondary mirror (SM). The instrument module contains the optics downstream of the tertiary mirror and the camera (detector). The sunshield is large, deployable and light-weight, thus accounting for the first flexible mode of the spacecraft structure around 0.2 Hz.

Integrated Modeling

The integrated model for NEXUS contains a structural finite element model (FEM), see Figure 24. The model was initially created in FEMAP/NASTRAN and subsequently translated to IMOS.²³ The figure shows the important locations at which disturbance and control inputs enter as well as important output nodes for the ACS as well as the locations where optical elements are mounted.

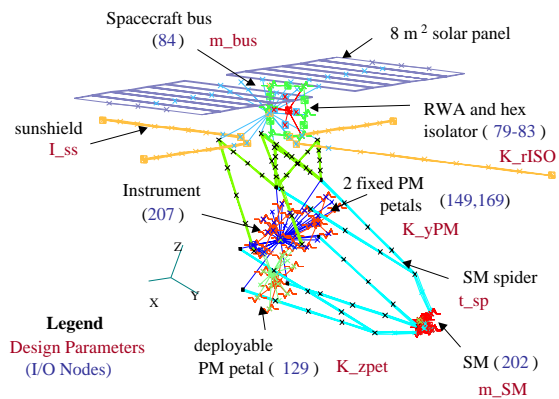


Fig. 24 NEXUS Finite Element Model. Important I/O grid points (nodes) and variable design parameters are shown.

The two performance metrics of interest are the root-mean-mean-square wavefront error, $J_{z,1} = \text{RMMS WFE}$, and the root-sum-square line-of-sight jitter, $J_{z,2} = \text{RSS LOS}$. The optical linear sensitivity matrices for these performance with respect to the translations and rotations of the optical elements were computed with MACOS. There are four expected disturbance sources in the model ($n_d = 4$). The first is broadband reaction wheel noise, assuming a 4-wheel pyramid and uniform probability density on the wheel speed distribution, with an upper (operational) wheel speed R_u . The disturbance forces and torques are caused by static and dynamic imbalances, U_s and U_d , as well as higher harmonics. The second disturbance is due to a linear Sterling cryocooler at drive frequency f_c . This device is used to cool the IR detector and is installed in the instrument module. The third disturbance is attitude noise, which is based on rate gyro noise and star tracker noise measured on the Cassini

mission (JPL). Finally there is guide star noise, which is very sensitive to the guider sampling rate, T_{gs} , and the guide star brightness, M_{gs} . The appended dynamics of this system are shown in the block diagram of Figure 25.

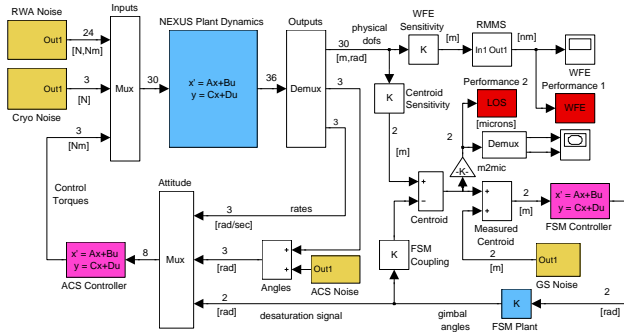


Fig. 25 NEXUS block diagram with 4 disturbance sources (RWA, Cryo, ACS noise, GS noise) and 2 performances (RMMS WFE, RSS LOS). Simulation implemented in Simulink as well as state space.

In summary the appended dynamics, S_{zd} , of this system contain 320 states ($n_s = 320$), two performance metrics ($n_z = 2$), four disturbance sources ($n_d = 4$) and 25 variable design parameters ($n_p = 25$). Table 3 summarizes the variable design parameters in the NEXUS case study.

Disturbance Analysis

A disturbance analysis was carried out with the initial parameters, p_o , given in Table 3. Results for LOS jitter are contained in Figure 26. The bottom plot shows a sample time realization for 5 seconds and the centroid X location. The middle plot shows the PSD of LOS jitter (RSS LOS) for a frequency domain and time domain calculation. The top plot is the cumulative RMS of LOS jitter as a function of frequency.

Another way to look at performance $J_{z,2}$ is to plot the time histories from the motions of centroid X and Y versus each other. This has been done in Figure 27. The predicted RSS LOS is $14.97 \mu m$, versus a requirement of $5 \mu m^5$.

The wavefront error performance is omitted here for simplicity, but is discussed by the author elsewhere.⁹ Table 4 shows an overview of the predicted performance, using the initial parameters p_o .

The wavefront error requirement ($\lambda/50$) is nearly met, but the pointing performance has to improve by a factor of roughly three.

Sensitivity Analysis

The next step is a comprehensive sensitivity analysis for the 25 variable design parameters of NEXUS. The sensitivity produces the normalized Jacobian matrix

⁵This requirement comes from the assumption of $25 \mu m$ pixel pitch and a desire to maintain LOS jitter below $1/5$ of a pixel.

Table 3 NEXUS Variable Design Parameters p_j , $j = 1, \dots, 25$.

Symbol	Nom	Description	Units
disturbance parameters			
Ru	3000	upr op wheel speed	[RPM]
Us	1.8	stat whl imbalance	[gcm]
Ud	60	dyn whl imbalance	[gcm ²]
fc	30	cryo drive freq	[Hz]
Qc	0.005	cryo attenuation	[-]
Tst	20	star track update	[sec]
Srg	3e-14	RG noise intensity	[rad ² /s]
Sst	2	Tracker one sigma	[arcsec]
Tgs	0.04	Guider int time	[sec]
plant parameter			
$m_s M$	2.49	mass of SM	[kg]
$K_y PM$	0.8e6	PM bipod stiffness	[N/m]
$K_r ISO$	3000	RW Isolator stiff	[Nm/rad]
$m_b us$	0.3e3	S/C bus mass	[kg]
$K_z pet$	0.9e8	petal hinge stiff	[N/m]
$t_s p$	0.003	Spider wall thick	[m]
$I_s s$	0.8e-8	SS bend inertia	[m ⁴]
$I_p ropt$	5.11	prop sys inertia	[kgm ²]
ζ	0.005	modal damping	[-]
optics parameters			
λ	1e-6	CL opt wavelength	[m]
Ro	0.98	opt surf trans	[-]
QE	0.80	CCD quantum eff	[-]
Mgs	15.0	mag of guide star	[mag]
controls parameters			
fca	0.01	ACS control BW	[Hz]
Kc	0.0	FSM/ACS coupling	[0-1]
Kcf	2000	FSM controller gain	[-]

evaluated at p^o

$$\bar{\nabla} J_z = \frac{p_o}{J_{z,o}} \begin{bmatrix} \frac{\partial J_{z,1}}{\partial R_u} & \frac{\partial J_{z,2}}{\partial R_u} \\ \dots & \dots \\ \frac{\partial J_{z,1}}{\partial K_{cf}} & \frac{\partial J_{z,2}}{\partial K_{cf}} \end{bmatrix} \quad (49)$$

which is graphically shown in Figure 28. Note that parameters Ru through Tgs are disturbance parameters, $m_s M$ through ζ are structural plant parameters, λ through Mgs are optical parameters and fca through Kcf are control parameters.

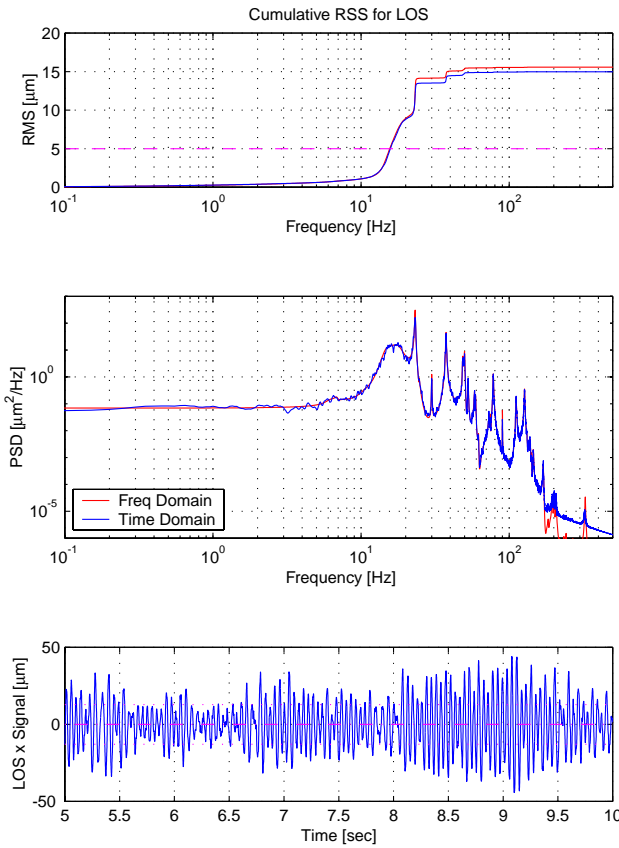


Fig. 26 LOS Jitter initial disturbance analysis

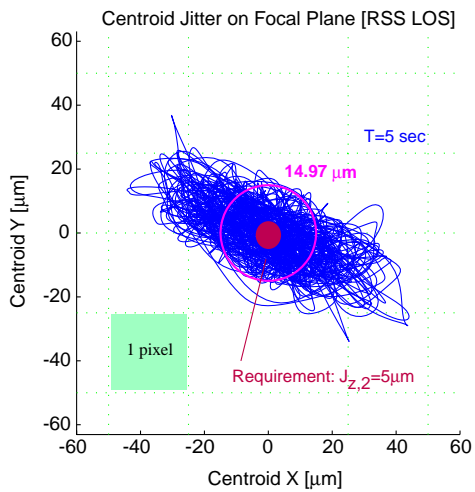


Fig. 27 RSS LOS Centroid Jitter Plot on Focal Plane

The RMMS WFE is most sensitive to the upper operational wheel speed, Ru , the RWA isolator stiffness, K_rISO , and the deployable petal hinge stiffness, K_zpet . The RSS LOS is most sensitive to the dynamic wheel imbalance, Ud , the RWA isolator stiffness, K_rISO , structural damping, $zeta$, the guide star magnitude, Mgs and the FSM (fine pointing loop) control gain, Kcf . Interpreting these results one would expect for example that a 1.0 % decrease in the

Table 4 Initial Performance Analysis Results

Performance	Lyap	Time	Req	Units
$J_{z,1}$ RMMS WFE	25.61	19.51	20	[nm]
$J_{z,2}$ RSS LOS	15.51	14.97	5	[μ m]

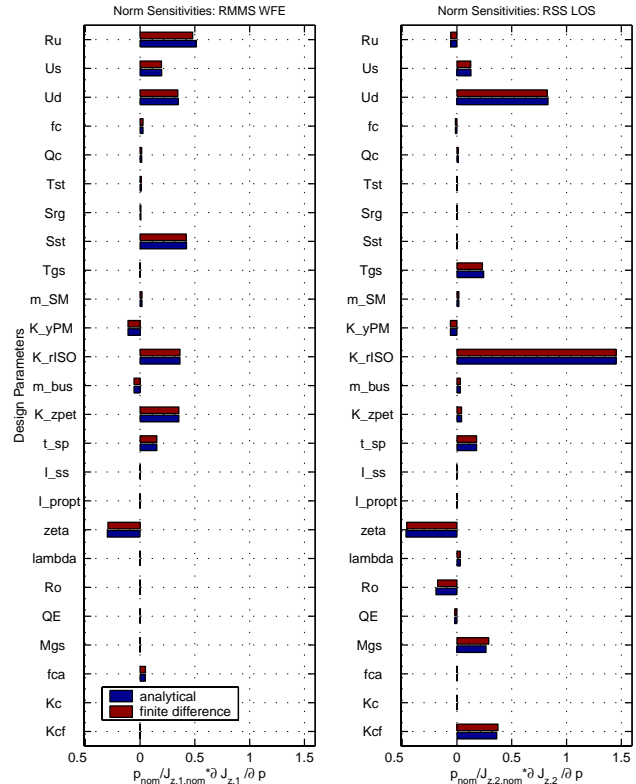


Fig. 28 NEXUS normalized sensitivity analysis results at p° .

isolator stiffness, K_rISO should lead to roughly a 1.5 % decrease in LOS jitter. The sensitivity analysis can be used to select a subset of interesting parameters for further analysis.

Bivariate Isoperformance

A bivariate isoperformance analysis is conducted for NEXUS using $J_{z,1} = \text{RSS LOS}$ as the performance and the two most sensitive parameters from Figure 28, right column, as the parameters. Hence, dynamic wheel imbalance, Ud , is traded versus RWA isolator joint stiffness, K_rISO , while constraining the performance the the requirement, $J_{z,2,req} = 5[\mu m]$. The results are contained in Figure 29.

The isoperformance contour at $\text{RSS LOS} = 5 \mu m$ can be reached from the initial design, p_o , by keeping the same amount of imbalance in the wheels (specification value of E-wheel: $U_d = 60 [\text{gcm}^2]$) and softening the isolator to below 1000 [Nm/rad], thus reducing the isolator corner frequency to roughly 1.2 Hz. Alternatively the isolator can remain the same and

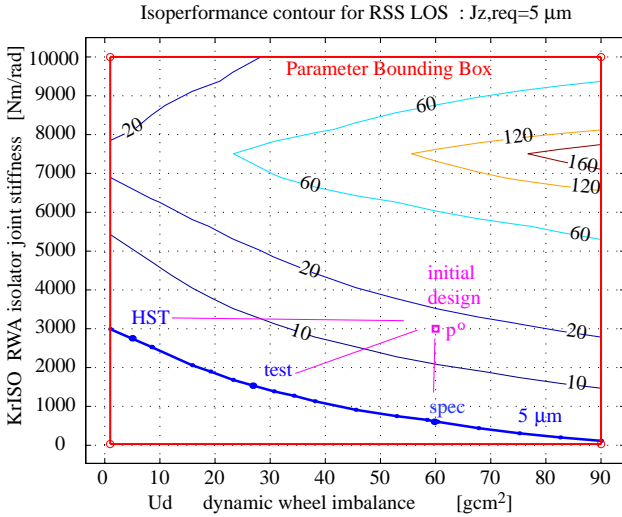


Fig. 29 NEXUS Bivariate Isoperformance analysis with $p_1 = U_d$, $p_2 = K_r ISO$ and $J_z = RSSLOSS$.

the imbalance could be reduced to close to its lower bound, $U_d=1$ [gcm²]. The isoperformance contour passes through these two points, so a combination of the above is likely to result in the desired effect. Note that the performance degrades significantly for stiffer isolator struts and larger imbalances. The region in the upper right of Figure 29, where LOS jitter of 160 μm is predicted, occurs, when the isolator modes coincide with other flexible modes of the NEXUS structure.

Multiobjective Optimization

Since solutions, p_{iso} , in the isoperformance set **I** do not distinguish themselves via their performance, we may satisfy some additional objectives. For the previous bivariate analysis for example it is not immediately clear whether it is more favorable or “expensive” to improve the balancing of the reaction wheels or to build a “softer” hexapod isolator. Once the (iso)performance requirements, $J_z(p_{iso}) = J_{z,req}$, are met one may consider competing cost objectives J_c (control effort, implementation cost, system mass, dissipated power, etc.) or risk objectives J_r (stability margins, sensitivity of performance to parametric uncertainty etc.). Which combination of J_c and J_r to use is application dependent. A non-linear optimization problem, given in (7) may be solved, whereby Q_{cc} and Q_{rr} are weighting matrices among the cost and risk objectives and η is used to trade between cost and risk. The result is a family of pareto optimal solutions, p_{iso}^* , which is presented to the designer.

Such a multivariable analysis was conducted for a subset of 10 out of the 25 design parameters for NEXUS. The two performance objectives RMMS WFE and RSS LOS were defined above. The cost and risk objectives are defined as follows:

- $J_{c,1}$ = Build-to Cost (closeness to “mid-range”)
- $J_{c,2}$ = Smallest FSM control gain
- $J_{r,1}$ = Percent performance uncertainty

The three pareto optimal solutions, which each individually optimize one of the above objectives, while meeting the isoperformance condition, are shown in the radar plot of Figure 30.

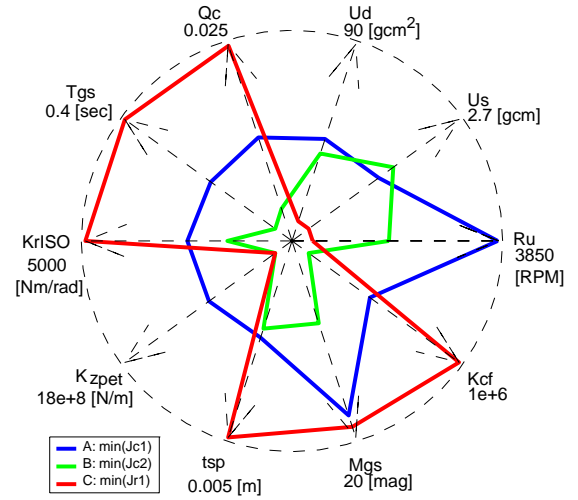


Fig. 30 NEXUS Multivariable Isoperformance. Radar plot of 3 pareto optimal designs.

Specifically, the isoperformance condition leads to the fact that all designs, p_{iso}^* , asymptote to the same value in the cumulative RMS plot, as shown for RSS LOS as shown in Chapter 7 of reference.⁹ The results for the NEXUS pareto optimal designs are summarized in Table 5.

Table 5 NEXUS pareto optimal designs

	$J_{z,1}$	$J_{z,2}$	$J_{c,1}$	$J_{c,2}$	$J_{r,1}$
A	20.0000	5.2013	0.6324	0.4668	± 14.3 %
B	20.0012	5.0253	0.8960	0.0017	± 8.8 %
C	20.0001	4.8559	1.5627	1.0000	± 5.3 %

Even though these designs achieve the same WFE and LOS jitter performance, this performance is achieved by placing the burden of different parts of the design.

7 Contributions and Recommendations

Contributions

This paper develops and validates a novel approach to the design of complex multi-disciplinary systems.

The isoperformance approach enhances the understanding of complex opto-mechanical systems by exploiting physical parameter sensitivity and performance information beyond the local neighborhood of a particular point design. The following specific contributions are identified:

- Developed a methodology for identifying the locus of parameters that yields constant performance levels of an LTI system.
- Applied isoperformance analysis to model-based error budgeting and multiobjective optimization for dynamic systems
- Produced and validated a software toolbox for conducting 2D or multivariable isoperformance analyses
- Experimental validation of isoperformance technique on a laboratory test article in 1-g with two parameters.

Limitations

The limitations of the isoperformance framework are that it assumes Linear-Time-Invariant (LTI) systems and operates on H2-performance metrics for zero-mean random processes. Furthermore the dynamics are treated in continuous time (no z-domain capability). The algorithms (except exhaustive search) require continuous and differentiable parameters and work within a given topology/architecture.

Recommendations

The recommendations for future work focus on removing some of the current limitations and applying the isoperformance concept on a more holistic level in product design and system architecture. Isoperformance meshes well with a product design philosophy called “satisficing”. In this approach not a product that optimizes the performance is sought, but rather a product that meets identified customer performance requirements, while being designed in a cost effective way.

Acknowledgments

This research was supported by the NASA Goddard Space Flight Center under contracts No. NAG5-6079 and No. NAG5-7839 and by the Jet Propulsion Laboratory under the SIM research contract No. JPL 961123. The above research contracts were monitored by Mr. Gary Mosier (GSFC), Dr. Sanjay Joshi (JPL) and Mr. Robert Grogan (JPL), respectively.

References

- ¹K. J. BATHE, *Finite Element Procedures*, Prentice-Hall, Inc., 1996.
- ²B. BIALKE, *A compilation of reaction wheel induced spacecraft disturbances*, in Proceedings of the 20th Annual AAS Guidance and Control Conference, Breckenridge, CO, February 5–9, 1997. AAS Paper No. 97-038.
- ³B. BIALKE, *A compilation of reaction wheel induced spacecraft disturbances*, 20th Annual American Astronautical Society Guidance and Control Conference, 1 (1997).
- ⁴R. G. BROWN AND P. Y. C. HWANG, *Introduction to Random Signals and Applied Kalman Filtering*, John Wiley & Sons, Inc., 1997.
- ⁵R. CRAIG JR., *Structural Dynamics: An Introduction to Computer Methods*, John Wiley & Sons, Inc., 1981.
- ⁶E. F. CRAWLEY, B. P. MASTERS, AND T. T. HYDE, *Conceptual design methodology for high performance dynamic structures*, in Proceedings of the 36th AIAA Structures, Structural Dynamics, and Materials Conference, New Orleans, LA, April 1995, pp. 2768–2787. AIAA Paper No. 95-2557.
- ⁷C. DE BOOR, *A practical guide to splines*, vol. I of Applied mathematical sciences, Springer Verlag, New York, 1 ed., 1978.
- ⁸O. L. DE WECK, *Integrated Modeling and Dynamics Simulation for the Next Generation Space Telescope*, master's thesis, Massachusetts Institute of Technology, June 1999.
- ⁹———, *Multivariable Isoperformance Methodology for Precision Opto-Mechanical Systems*, PhD thesis, Massachusetts Institute of Technology, Department of Aeronautics and Astronautics, 2001.
- ¹⁰A. DRESSLER, *HST and Beyond - Exploration and the Search for Origins: A Vision for Ultraviolet-Optical-Infrared Space Astronomy*, vol. 1, Association of Universities for Research in Astronomy, Washington D.C., 1 ed., May 1996.
- ¹¹C. H. EDWARDS AND D. E. PENNEY, *Multivariable Calculus with Analytic Geometry*, Prentice Hall, Upper Saddle River, NJ 07458, 5 ed., 1998.
- ¹²C. E. EYERMAN AND J. F. SHEA, *A systems engineering approach to disturbance minimization for spacecraft utilizing controlled structures technology*, MIT SERC Report #2-90, June 1990.
- ¹³R. L. FOX AND M. P. KAPOOR, *Rates of change of eigenvalues and eigenvectors*, AIAA Journal, 6 (1968), pp. 2426–2429.
- ¹⁴P. R. FREUND, *Course Notes 16.910J/6.631 - Introduction to Simulation and Optimization - Massachusetts Institute of Technology*. Module 1, Sep-Oct 1999.
- ¹⁵J. J. GILHEANY, *Optimum selection of dampers for freely vibrating multidegree of freedom systems*, Proceedings of Damping '89, II (1989), pp. FCC-1:18.
- ¹⁶O. GOLDREICH, *Complexity theory survey*. Internet: <http://www.wisdom.weizmann.ac.il>, accessed 5-4-2001 2001.
- ¹⁷C. Z. GREGORY, *Reduction of large flexible spacecraft models using internal balancing theory*, Journal of Guidance, Control, and Dynamics, 7 (1984), pp. 17–32.
- ¹⁸H. L. GUTIERREZ, *Performance Assessment and Enhancement of Precision Controlled Structures During Conceptual Design*, PhD thesis, Massachusetts Institute of Technology, Department of Aeronautics and Astronautics, 1999.
- ¹⁹G. J. HOU AND S. P. KENNY, *Eigenvalue and eigenvector approximate analysis for repeated eigenvalue problems*, AIAA Journal, 30 (1992).
- ²⁰G. J. HOU AND G. KOGANTI, *Sensitivity analysis of Lyapunov and Riccati equations with application to controls-structures integrated design*, in Proceedings of the 34th AIAA/ASME/ASCE/AHS/ASC Structures, Structural Dynamics and Materials Conference, LaJolla, CA, April 1993, pp. 1906–1915. AIAA Paper No. 93-1529.

- ²¹R. N. JACQUES, *An approach to the preliminary design of controlled structures*, master's thesis, Massachusetts Institute of Technology, February 1991. SERC Report #1-91.
- ²²JET PROPULSION LABORATORY, *Modeling and Analysis for Controlled Optical Systems User's Manual*, 1997.
- ²³———, *Integrated Modeling of Optical Systems User's Manual*, January 1998. JPL D-13040.
- ²⁴H. R. JR., *Multivariable Calculus with Vectors*, Massachusetts Institute of Technology, Prentice Hall, Upper Saddle River, New Jersey 07458, 1999.
- ²⁵M. P. KAMAT, *Structural Optimization: Status and Promise*, vol. 150 of Progress in Aeronautics and Astronautics, American Institute of Aeronautics and Astronautics, Washington, D.C., 1992.
- ²⁶S. KENNY, *Eigenvalue and eigenvector derivatives for structures*, Final Report, MIT Course 2.093: Computer Methods in Dynamics, April 29, 1997.
- ²⁷R. A. LASKIN, *SIM Dynamics & Control Requirements Flowdown Process*. Presentation at the SIM Project Preliminary Instrument System Requirements Review, JPL, March 17–18, 1998.
- ²⁸R. A. LASKIN AND M. SAN MARTIN, *Control/structure system design of a spaceborne optical interferometer*, in Proceedings of the AAS/AIAA Astrodynamics Specialist Conference, Stowe, VT, August 1989. AAS Paper No. 89-424.
- ²⁹A. LAUB, *Computation of balancing transformations*, Proceedings of JACC, 1 (1980).
- ³⁰A. LAUB, M. HEATH, C. PAIGE, AND R. WARD, *Computation of system balancing transformations and other applications of simultaneous diagonalization algorithms*, IEEE Trans. Automatic Control, (1987), pp. 115–122.
- ³¹G. MALLORY AND D. W. MILLER, *Decentralized state estimation for flexible space structures*, 40th AIAA Structural Dynamics and Materials Conference, (1999).
- ³²G. J. MALLORY, *Development and Experimental Validation of Direct Controller Tuning for Spaceborne Telescopes*, PhD thesis, Massachusetts Institute of Technology, Department of Aeronautics and Astronautics, April 2000. Report SERC 1-2000.
- ³³B. P. MASTERS AND E. F. CRAWLEY, *Evolutionary design of controlled structures systems*, in Proceedings of the 38th AIAA Structures, Structural Dynamics, and Materials Conference, Kissimmee, FL, April 1997. AIAA Paper No. 97-1263.
- ³⁴A. MESSAC, R. GUELER, AND K. MALEK, *Control-structure integrated design: A computational approach*, in Proceedings of the 32nd AIAA/ASME/ASCE/AHS/ASC Structures, Structural Dynamics, and Materials Conference, Baltimore, MD, April 1991, pp. 553–567. AIAA Paper No. 91-1161.
- ³⁵D. MILLER, A. CURTIS, AND O. DE WECK ET AL., *Architecting the search for terrestrial planets and related origins (astro)*, in SPIE International Symposium on Astronomical Telescopes and Instrumentation 2000, Munich, Germany, 2000.
- ³⁶D. MILLER, O. DE WECK, S. UEBELHART, R. GROGAN, AND I. BASDOGAN, *Integrated dynamics and controls modeling for the space interferometry mission (sim)*, in IEEE Aerospace Conference, Big Sky, Montana, 2001.
- ³⁷M. MILMAN, M. SALAMA, R. SCHEID, R. BRUNO, AND J. GIBSON, *Integrated control-structure design: A multiobjective approach*, Tech. Report D-6767, JPL, October 1989.
- ³⁸M. MILMAN, M. SALAMA, R. SCHEID, AND J. S. GIBSON, *Combined control-structural optimization*, Computational Mechanics, (1991), pp. 1–18.
- ³⁹M. MILMAN, M. SALAMA, M. WETTE, AND R. BRUNO, *A multiobjective approach to integrated control, structure and optical design*, in Proceedings of the 32nd AIAA/ASME/ASCE/AHS/ASC Structures, Structural Dynamics, and Materials Conference, Baltimore, MD, April 1991, pp. 846–854. AIAA Paper No. 91-1136.
- ⁴⁰B. C. MOORE, *Principal component analysis of linear systems: Controllability, observability, and model reduction*, IEEE Transactions on Automatic Control, AC-26 (1981), pp. 17–32.
- ⁴¹D. V. MURTHY AND R. T. HAFKA, *Survey of methods for calculating sensitivity of general eigenproblems*, in Sensitivity Analysis in Engineering, Langley Research Center, September 1986, pp. 177–196. NASA CP 2457.
- ⁴²R. B. NELSON, *Simplified calculations of eigenvector derivatives*, AIAA Journal, 14 (1976), pp. 1201–1205.
- ⁴³S. L. PADULA, B. B. JAMES, G. P. C., AND S. E. WOODARD, *Multidisciplinary optimization of controlled space structures with global sensitivity equations*, Tech. Report NASA TP-3130, National Aeronautics and Space Administration, November 1991.
- ⁴⁴C. G. PARK AND D. W. MILLER, *Structural design and control of high performance optical delay lines*, master's thesis, Massachusetts Institute of Technology, Department of Aeronautics and Astronautics, August 1995.
- ⁴⁵J. I. PRITCHARD, H. M. ADELMAN, AND J. SOBIESZCZANSKI-SOBIESKI, *Optimization for minimum sensitivity to uncertain parameters*, AIAA Journal, 34 (1996), pp. 1501–1504.
- ⁴⁶D. C. REDDING AND W. G. BRECKENRIDGE, *Optical modeling for dynamics and control analysis*, Journal of Guidance, Control, and Dynamics, 14 (1991), pp. 1021–1032.
- ⁴⁷M. B. J. ROBERT S. KENNEDY AND D. R. BALTZLEY, *Empirical demonstration of isoperformance methodology preparatory of an interactive expert computerized decision aid. final report*, Tech. Report AIAA Technical Library, NTIS HC A03/MF A01, Essex Corporation, Orlando, FL, Feb 1988. AD-A202439; ARI-RN-88-93; Contract: MDA903-87-C-0603; Contract: DA PROJ. 2Q6-65502-M-770.
- ⁴⁸M. B. J. ROBERT S. KENNEDY AND D. R. BALTZLEY, *Optimal solutions for complex design problems: Using isoperformance software for human factors trade offs*, In NASA. Lyndon B. Johnson Space Center, 2nd Annual Workshop on Space Operations Automation and Robotics (SOAR 1988), N89-19817 12-59 (1988), pp. 313–319.
- ⁴⁹J. T. R.S. KENNEDY AND M. B. JONES, *A meta-model for systems development through life cycle phases - coupling the isoperformance methodology with utility analysis*, SAE, Aerospace Technology Conference and Exposition, Long Beach, CA, AIAA Technical Library (1990), p. 9.
- ⁵⁰J. SPANOS, Z. RAHMAN, AND G. BLACKWOOD, *A soft 6-axis active vibration isolator*, in Proceedings of the American Control Conference, Seattle, WA, June 1995.
- ⁵¹G. STRANG, *Introduction to Applied Mathematics*, Wellesley-Cambridge Press, 1986.
- ⁵²J. VAN DE VEGTE, *Feedback Control Systems*, Prentice-Hall, Inc., 1990.
- ⁵³S. L. VENNARI, *Future directions and needs in engineering tools*, ICASE/LARC/NSF/ARO Workshop on Computational Aerosciences in the 21st Century, (1998). Hampton, Virginia.
- ⁵⁴M. WEHNER, *Personal Communication, TRW, Redondo Beach, CA*, 1999.
- ⁵⁵W. T. V. WILLIAM H. PRESS, SAUL A. TENKOLSKY AND B. P. FLANNERY, *Numerical Recipes in C - The Art of Scientific Computing*, Cambridge University Press, 2nd ed., 1996.
- ⁵⁶P. H. WIRSCHING, T. L. PAEZ, AND H. ORTIZ, *Random Vibrations: Theory and Practice*, John Wiley & Sons, Inc., 1995.
- ⁵⁷H. N. YOSHIKAZU SAWARAGI AND T. TANINO, *Theory of Multiobjective Optimization*, vol. 176 of Mathematics in Science and Engineering, Academic Press Inc., London, United Kingdom, 1 ed., 1985.
- ⁵⁸K. ZHOU, J. C. DOYLE, AND K. GLOVER, *Robust and Optimal Control*, Prentice-Hall, Inc., 1996.